SIMULATION OF TRANSPORT PHENOMENA DURING PHASE CHANGE IN CONTINUOUS CASTING OF STEEL

by

Peter Tong-Kan YU

A thesis submitted to the School of Graduate Studies in partial fulfillment of the requirements of the degree of

MASTER OF APPLIED SCIENCE

in the

Department of Mechanical Engineering
University of Ottawa
Ottawa, Canada
1985

UNIVERSITÉ D'OTTAWA
UNIVERSITY OF OTTAWA

ACKNOWLEDGEMENT

I wish to express my gratitude to my supervisor, Dr. Martha Salcudean, for her invaluable suggestion, constant encouragement, and hearty inspiration throughout the research. I am also indebted for her careful checking of this manuscript.

Indebtness is also due to Dr. Mark Lai for his constant support and interest in my study and in the development of the multi-phase computer code. Thanks are also due to him for always finding time, either in the office or in his home to share his expertise with me.

The financial support received from my supervisor, the Natural Science and Engineering Research Council and the University of Ottawa is gratefully acknowledged.

I wish to express my sincere admiration to Miss Louisa Tsui for her patience and diligence in preparing the typescript of the thesis. Thanks are also due to Henry Knoll for his proof reading of the manuscript.

Last but not least, I also wish to thank my family and friends for their moral support and encouragement.

ABSTRACT

The present study is aimed at simulating the transport phenomena of multi-phase flow with phase change, as applied to the process of continuous casting of steel.

A generalized mathematical model is formulated to describe the transport phenomena inside a "multi-phase domain".[1] Heat and mass transfer mechanisms considered are the buoyancy and forced convection, conduction and turbulent fluid flow. A novel phase change (latent heat) treatment is also proposed.

Based on the finite volume method (FVM), a new discretization method of the partial differential equations (PDE)s is developed. Two new numerical solution algorithms are also developed for:

a) solving the energy equation with phase change,

b) tracing the unknown location of the boundary between phases (interface line).

The overall solution procedure for the equation of motion is based on the SIMPLE algorithm [35].

---

[1] In the present study, the term "Multi-phase Domain" is used to represent a domain which consists of multi-distinct phase regions separated by the interface boundaries.

The formulated mathematical model and the whole numerical solution procedure were applied to a number of model problems. Computed values of solid fraction distributions and fluid flow patterns, have been found to agree satisfactorily with the available experimental data.

CONTENTS

LIST OF TABLES

LIST OF FIGURES

NOMENCLATURE

Symbols	Definition
A	Area
a	Coefficients in the algebraic equation for the line solution procedure
C	Convective transport across cell-boundary ($= \rho u$)
C_1, C_2	Constants in the modelled ϵ-equation
C_μ	Constants in the effective viscosity expression
C_D	Constants in the dissipation terms of the k-equation
C_p	Specific heat of fluid.
D	Diffusive transport across cell-boundary ($= \Gamma/L$)
E	Emissitivity
F	View factor
f_s	Solid fraction
G	Generation of turbulence energy
g	Gravitional acceleration
h	specific enthalpy
H	Local enthalpy
k	Turbulence kinetic energy ($= 1/2\ \overline{u_i u_j}$)
K	Thermal conductivity
P	Local pressure
P"	Reduced Pressure ($= P - \rho_L\ g\ x$)
Pe	Peclet number ($= \rho u L / \Gamma$)
Pr	Prandtl number ($= C_p \mu / \lambda$)
Q	Total transport across cell-boundary
r	Radius

r_L	Radius of liquidus line
r_S	Radius of solidus line
R_{mold}	Radius of the mold
Re	Reynolds number (= $U\Delta r$ / υ)
S	Source term in the conservation equation
T	Local fluid temperature
t	Time
U, V	Mean velocity component in the x- and r-direction respectively in cylindrical coordinates; mean velocity component in the x- and y-direction respectively in rectangular coordinates
u, v	Velocity fluctuation component in the x- and y-direction respectively
Vol	Cell volume
x, r	General cylindrical coordinates

Greek Symbols	Definition
ε	Dissipation rate of turbulence kinetic energy
Γ_h, Γ	Exchange coefficient (= μ / σ)
Γ_t	Turbulent diffusivity
μ	Dynamic viscosity
υ	Kinematic viscosity
ζ	Symbols for different phases
ρ	Fluid density
ϕ	General variable
σ	Prandtl number (= $C_p\mu/\lambda$)
σ_k	Constant in modelled k-equation
σ_ε	Constant in modelled ϵ-equation

γ	Dimensionless area ratio
θ	Dimensionless volume ratio
β	Thermal expansion coefficient
Σ	Summation
ψ	Stream function
$\delta x, \delta y$	Distance between two adjacent grid points
$\Delta x, \Delta y$	Width of the control volume

<u>Subscripts</u>	<u>Definition</u>
i,j	General nodal point (i,j)
eff	Effective value
inlet	For inlet boundary
L	At Liquidus
l	Liquid region
m	Mushy region
mo	At mold
nor	Normalized value
N,S,E,W	Point of compass notation for grid point value
n,s,e,w	Point of compass notation for grid boundary value
nb	General neighbouring grid point
noz	At nozzle
outlet	For outlet boundary
P	Central grid point of interest
S	At Solidus
so	Solid region
t	Turbulent

wall	At wall

Superscripts	Definition
'	Fluctuating component; correction value
--	Average value
*	Guessed value
eff	Effective mean value
i	Imposed value
o	Old iteration value

Abbreviatios	Definition
FVM	Finite Volume Method
MAX	Maxium value
MIN	Minium value
PDE	Partial Differential Equation

CHAPTER 1

INTRODUCTION

1.1 BACKGROUND

The purpose of the present study is to develop a model simulating the transport phenomena involved for a multi-phase domain with phase change.

Both multi-phase flow and phase change are of considerable practical importance in industrial processes. For example:

(i) Processes involving phase change only, such as liquid-solid phase change during solidification and solid-liquid phase change during melting of pure substances.

(ii) Processes involving multi-phase flow only, such as the metallurgical process of argon gas stirred ladle in which there is an argon gas-steel two-phase region.

(iii) Processes involving both phase change and multi-phase flow, such as :

a) coolant around a reactor bundle, in which there is a liquid-vapor two-phase region and vaporization takes place.

b) solidification of an alloy, in which there is a liquid-solid two-phase region and latent heat of fusion is released during the liquid-solid phase change. Conversely, latent heat is absorbed during melting.

1.2 PRACTICAL RELEVANCE OF CONTINUOUS CASTING OF STEEL

1.21 DESCRIPTION OF THE PROCESS

Figure 1.21-1 shows a simplified schematic diagram of the continuous casting[2] of a cylindrical mold. In continuous casting, liquid steel from the tundish is poured continuously into the water-cooled mold. Though solidification a shell forms along the periphery and grows towards the centre. Once the casting emerges from the mold, it is further cooled by spraying water directly on the outer surface of the solidified metal. At the end of water spray cooling, when most of the liquid steel has solidified, heat is lost by radiation. (For detail, see ref. F. Weinberg 1975 [56], H.E. Allen st al 1977 [2], C.H. Bode 1977 [6])

---

[2] As the name indicates, continuous casting is an operation where the metal continuously solidifies (see ref. Bode 1977 [6]).

1.22 IMPORTANCE OF CASTING SIMULATION

The solidification process that takes place in a continuous casting system involves many complex phenomena, as shown in Fig. 1.22-1. In the present study, the whole process is assumed to involve three distinct phase regions; namely, liquid, solid, and mushy[3], separated by two non-straight phase lines. There are forced and natural convective effects in the liquid region; there is conductive heat transfer in the solid region; and in the mushy region, there are phase change, two-phase effects, interface effects and all previously mentioned phenomena. Heat exchange at the boundaries involves different mechanisms, such as radiation, conduction, and nucleate boiling.

Studies have shown (see ref. F. Weinberg 1974 [56]) that the formation of defects during the solidification can be explained and partly corrected by controlling the casting process parameters. For example, the central porosity produced by the shrinkage of the metal at the completion of solidification is affected mainly by the casting temperature and the withdrawal rate. Flow pattern (see ref. Asai et al 1975 [4], Szekely et al 1978 [47]) in the pool of molten steel is believed to have a significant effect on the

---

[3] The term "mushy region" is used to represent a region in which latent heat of fusion is liberated and in which liquid and solid phases co-exist.

quality of the cast products, since some flow patterns are more favorable to floatation of the non-metallic inclusions up to the metal-slag interface.

Therefore, a proper quantitative and qualitative description of the transport phenomena, such as flow patterns and temperature distributions, is a necessary prerequisite for seeking process optimization.

1.3 MOTIVATION OF PRESENT STUDY

1.31 BACKGROUND

Problems in a situation consisting of different phase regions with two-phase flow and phase change phenomena are in general complex processes, as noted in subsection 1.22. There are numerous parameters and the individual or combined effects of each parameter is difficult to evaluate. Hence, most problems are impossible to solve analytically in closed forms.

1.32 EXPERIMENTAL DIFFICULTIES

Difficulties are also encountered in experimental work because quantitative results are usually very hard, expensive or time-consuming to obtain. For instance, Vandrunen and Brimacombe [53], Lait 1975 [24], Morton and Weinberg 1973 [34], examined the shell thickness and pool depth of castings by the addition of a radioactive tracer of gold to the molten pool, followed by autoradiographs of the sectioned casting. It is difficult to achieve all the conditions of a real metallurgical process of casting in a laboratory model; for example, Weinberg 1975 [56] concluded that because of substantially different behaviours and values in thermal conductivities between water and metals, a water model cannot be used to simulate fluid flow resulting from thermal gradients in castings. Direct measurements of fluid flow of molten steel are difficult because the steel is opaque and at high temperature.

1.33 MATHEMATICAL MODELLING

During solidification, the phase change phenomena, the turbulent transport of momentum and energy, are complex processes occurring in different phases. In modelling the multi-phase and phase change problem, many previous studies used assumptions based on extensive simplifications of the problem.

The mathematical problem is greatly simplified by assuming that fluid flow is unlikely to play a major role in affecting the rate of solidification, and thus its effect is neglected. This assumption is crude and contrary to the experimental findings (see ref. Stewart and Weinberg 1972 [46], Szekely and Todd 1971 [49]). Earlier studies by Savage 1952 [42], Hills 1965 [18], and Pehlke 1964 [38], simplified the problem further by assuming constant thermophysical properties. This simplification can introduce considerable uncertainty into the validity of the model.

Mizika 1967 [31] presented a model with variable thermophysical properties, such as thermal conductivity and specific heat. However in this model, only unidimensional heat transfer along the cross-section of the casting was considered (see also Kung and Pollock 1967 [22] and Lait and Brimacombe 1974 [24]).

For the treatment of latent heat, Hills 1965-69 [16-17], Moriyama and Muchi 1969 [33] presented only the profiles of the solidus[4] line based on the assumption that the latent heat of fusion is released at the solidus line. Miyazawa and Muchi 1975 [30] improved the model by assuming the existence of a mushy (liquid-solid two-phase) region, in which the latent heat of fusion is released. Furthermore, solid fraction treatment was also proposed.

---

[4] Solidus is the temperature at which the metal is completely solidified and the latent heat of fusion has been completely released.

For a more realistic thermal analysis, convective transport in the energy equation should also be considered. Mizika 1967 [31] and Brimacombe et al 1974 [24] have assumed that turbulent diffusion in the mold region was represented by an artificially high "effective" value for the thermal conductivity of the molten steel. Peel and Pengelly 1970 [37] have shown that this assumption does not fully reflect the physical phenomena for steel. Brody and Stoehr 1980 [7], Weckman et al 1979 [56] have taken the convective transport in the energy equation into account for simplified hydrodynamic conditions only, such as zero flow in cross-sectional direction and constant velocity in the main stream direction.

Considering both the fluid flow and thermal analysis tends to provide a much more accurate representation of the actual casting systems, although such an approach may pose a more complex mathematical task.

Yadoya and Szekely 1972 [48] provided the first attempt in modelling the transports in the mold section only. They assumed for their model that the thickness of the solidified layer in the upper mold region can be neglected. Hence, this model cannot be extended to simulate other parts of the casting domain.

Asai and Szekely 1974 [4] improved the model so that it could be applied to the whole system. However, the study assumed constant thermophysical properties, which in reality are usually a function of the temperature and phases involved in all different phase regions. Furthermore, the buoyancy effect on the flow field was neglected in the analysis. Finally, one of the most important conditions, the compatibility of variables, such as temperature and velocities along the interface lines, was not considered.

1.34 NUMERICAL SOLUTION

In theory the above multi-phase mathematical problem can be solved either by analytical or numerical approach. An analytical approach to the problem is certainly the more elegant of the two, but because of the complexity of the problem it is almost impossible to achieve (see attempts by Savage 1962 [42], Hills 1965 [18] and Pehlke 1964 [38]).

On the other hand, numerical approaches, which are considerably more versatile, appear to be better suited for solving solidification problems. Complex variations in the boundary conditions and variable thermophysical properties can be handled readily.

Different numerical techniques, such as finite difference method (see ref. Yadoya and Szekely 1972 [48], Asai et al 1975 [4], Lait and Brimacombe 1974 [24]) and finite element method (see ref. Brody et al 1980 [7], Weckman et al 1979 [55]), have been used to simulate the casting processes. However, these studies are based on one phase control volume, and this assumption can introduce errors in the interface tracing. Hence, a reformulation has been proposed in the numerical solution procedure in order to model the above multi-phase complex processes.

1.4 THE PRESENT CONTRIBUTION

The aim of the present study is to develop a model simulating the transport phenomena of multi-phase flow with phase change.

A mathematical model has been formulated to describe the transport phenomena inside a multi-phase domain. Turbulent fluid flow with buoyancy, heat and mass transfer are considered for different phase regions involved. In terms of the phase change phenomenon, a novel latent heat treatment, with no assumption of a heat release profile, is proposed.

A new discretization method based on the finite volume method (FVM) has been developed to discretize the governing multi-phase partial differential equations (PDE)s. New solution algorithms have also been developed; (1), to solve the energy equation with phase change, and (2), to trace the unknown location of the interface lines. The solution algorithm for the equations of motion based on the SIMPLE algorithm [35] has been developed.

In the present study the mathematical model and numerical solution procedures have been applied to a number of model cases for the process of continuous casting of steel in systems of cylindrical configurations.

1.5 OUTLINE OF THE THESIS

The thesis consists of five chapters. Chapter 2 deals with the mathematical modelling. The newly developed discretization method and all the solution procedures are presented in Chapter 3. Chapter 4 illustrates some aspects of the model performance. Finally Chapter 5 summarizes the results of the studies and makes recommendations for further work.

CHAPTER 2

MATHEMATICAL PROBLEM

2.1 INTRODUCTION

In this chapter the physical model describing the transport phenomena for the present studies is presented.

2.11 OUTLINE OF THE CHAPTER

First, the ensemble-averaged differential equations are derived for the velocity components, pressure, enthalpy (temperature) and other related scalar variables. In subsection 2.21 the instantaneous equations describing the turbulent flow are introduced in Cartesian tensor notation. The following subsection 2.22 is concerned with recasting these equations in terms of the ensemble-averaged quantities. The assembly of the differential equations is completed by using the k-ϵ turbulent viscosity model, and then a general form of the differential equations is presented in the cylindrical coordinate system. The interface conditions are discussed in section 2.3.

Finally, the physical model is closed in section 2.4 by consideration of the boundary conditions and the thermophysical properties.

2.12 DESCRIPTION OF THE PHYSICAL MODEL

In order to model the problem as shown in Fig. 1.22-1 in a mathematically manageable way, certain assumptions have to be made in the derivation of the fundamental equations. The assumptions are as follows:

1. The problem domain is considered to involve three distinct phase regions, namely liquid, solid and mushy.
2. A cylindrical co-ordinate system is used in describing the problem, which is axisymmetrical.
3. A homogenized flow, using the concept of solid fraction to describe the two-phase behaviour, is assumed in the mushy region.
4. The solid fraction is assumed to be a linear function of temperature.
5. Thermophysical properties in the mushy region depend on solid fraction (see subsection 2.41b for details).
6. Thermophysical properties vary in each phase region the (see subsection 2.41a for detail).
7. Incompressible, non-reacting, steady transport is occurring in all regions.

2.2 GOVERNING DIFFERENTIAL EQUATIONS

In this section the equations for the instantaneous conservation, the ensemble-averaged, and the k-ϵ turbulent viscosity model are presented.

2.21 INSTANTANEOUS CONSERVATION EQUATIONS

The fundamental equations presented here are equally applicable to describe the general, incompressible, non-reacting steady transport in all three regions (liquid, solid and mushy). In the Cartesian tensor notation, the differential equations for mass, momentum, and energy are given as follows (see, ref. Bird et al [5]):

Mass Conservation Equation

$$\partial(\rho u_j) / \partial x_j = 0 \qquad (2.21\text{-}1)$$

Momentum Conservation Equation

$$\partial(\rho u_j u_i) / \partial x_j - \partial(\Gamma \partial u_i/\partial x_j) / \partial x_j = -\partial P / \partial x_i + s_{u_i} \qquad (2.21\text{-}2)$$

Energy Conservation Equation

$$\partial(\rho u_j h) / \partial x_j - \partial(\mu/\sigma_h \partial h/\partial x_j) / \partial x_j = s_h \qquad (2.21\text{-}3)$$

where s_{u_i} and s_h are volumetric rates of body forces and energy generation/dissipation respectively. They also generally contain terms arising from the effects of non-uniformities in fluid properties, compression, etc. Also,

x_j = the three coordinates of the Cartesian system
u_j = the three components of the velocity vector
μ = the viscosity
P = pressure
ρ = density
h = specific stagnation enthalpy ($h=C_pT$, C_p is a constant pressure specific heat capacity and T is temperature)
σ_h = the Prandtl number for the energy equation.

Similar differential equations in cylindrical coordinates system are shown in subsection 2.24.

2.22 ENSEMBLE-AVERAGED EQUATIONS

In spite of recent advances in the direct solution of the time-dependent Navier-Stokes equations and in large-eddy simulation techniques (see, ref. Rogallo and Moin [41]), the only economically feasible way to solve practical turbulent flow problems is still the use of statistically averaged equations governing ensemble-averaged flow quantities, as illustrated in the following:

In an averaging operation, the instantaneous values of any variable f can be split as the sum of an ensemble-averaged component F plus a turbulent fluctuating component f' (see, ref. Townsend [51]):

$$f = F + f' \qquad (2.22\text{-}1)$$

where

$$F = \lim_{(t1-t2) \to \infty} [1/(t1-t2)] \int_{t2}^{t1} f(x_i, t)\, dt \qquad (2.22\text{-}2)$$

By applying the averaging procedure to instantaneous equations 2.21-1 to 2.21-3, the corresponding ensemble-averaged equations can be obtained. These ensemble-averaged equations are similar to the instantaneous ones except for the averaged momentum equations which contain additional turbulent or Reynolds stresses $(-\bar{\rho}\overline{u_i' u_j'})$, except for the averaged energy equation which contains additional turbulent heat or mass flux $(-\bar{\rho}\overline{u_i' h'})$. (Note that the superbar denotes the ensemble-averaged value.) Because of the appearance of these terms, the ensemble-averaged flow equations are not closed. To allow for solving these equations, those terms must be related to known or calculable quantities.

Following the normal practice (Launder and Spalding [25]), the additional terms are modelled as diffusion processes in order to make the ensemble-averaged equations similar in appearance to the equations for laminar flow. Hence, the additional terms are expressed in terms of gradients of ensemble-averaged quantities.

$$-\bar{\rho}\overline{u_j^{\prime}u_i^{\prime}} = \mu_t(\partial U_i/\partial x_j + \partial U_j/\partial x_i) \qquad (2.22\text{-}3)$$

$$-\bar{\rho}\overline{u_j^{\prime}h^{\prime}} = \mu_t/\sigma_{h,t}\ \partial H/\partial x_j \qquad (2.22\text{-}4)$$

where μ_t = turbulent viscosity

$\sigma_{h,t}$ = turbulent Prandtl number

Thus, the modelled forms of the ensemble-averaged conservation equations can be written as follows:

<u>Mass Conservation Equation</u>

$$\partial(\bar{\rho}U_j)/\partial x_j = 0 \qquad (2.22\text{-}5)$$

<u>Momentum Conservation Equation</u>

$$\partial[\bar{\rho}U_jU_i - (\mu+\mu_t)\partial U_i/\partial x_j]/\partial x_j - S_{U_i} = 0 \qquad (2.22\text{-}6)$$

<u>Energy Conservation Equation</u>

$$\partial[\bar{\rho}U_jH - (\mu/\sigma_h + \mu_t/\sigma_{h,t})\partial H/\partial x_j]/\partial x_j - S_H = 0 \qquad (2.22\text{-}7)$$

where S_{U_i} and S_H are the resultant ensemble-averaged source terms.

2.23 TURBULENCE MODELLING

a. Introductory Remarks

The turbulent viscosity μ_t is not a property of the fluid but is strongly position-dependent and largely determined by the nature of turbulence. The development of a correct, or at least acceptable, expression for μ_t is perhaps the most crucial factor in any predictive model for a turbulent system. In a recent book by Rodi 1980 [40], a review of the various turbulent models available for evaluating μ_t has been presented.

In the present study, a simple form of the k-ϵ Turbulent Viscosity Model (Jones and Launder [21]) is selected for evaluating the turbulent viscosity as part of a computational scheme for turbulent fluid flow calculations.

b. k-ϵ Turbulent Viscosity Model

Detailed description of the model is not presented here, only the turbulent viscosity expression and the ensemble-averaged equations for k and ϵ are given.

$$\mu_t = \rho \, c_\mu \, k^2/\epsilon \tag{2.23-1}$$

where k = turbulent kinetic energy

$= 1/2 \, (\bar{u}_i^T \bar{u}_i^T)$

ϵ = dissipation rate of turbulent kinetic energy

$$= (\mu/\bar{\rho})(\partial\bar{u}^{\tau}/\partial x_j)^2$$

Turbulent Kinetic Energy Equation

$$\partial(\rho U_j k - \mu_t/\sigma_k\ \partial k/\partial x_j)/\partial x_j - G + \rho\epsilon = 0 \qquad (2.23\text{-}2)$$

Dissipation Rate Equation

$$\partial(\rho U_j \epsilon - \mu_t/\sigma_\epsilon\ \partial\epsilon/\partial x_j)/\partial x_j - (Ge)\epsilon/k = 0 \qquad (2.23\text{-}3)$$

where $G = \mu_t(\partial U_i/\partial x_j)[\partial U_i/\partial x_j + \partial U_j/\partial x_i]$ (2.23-4)

$$Ge = C_1 G - C_2 \rho\epsilon \qquad (2.23\text{-}5)$$

C_μ, C_1 and C_2 are empirical constants determined from experiments (see Launder and Spalding [26]). The values used for the present studies are given in Table 2.1.

2.24 GENERAL TRANSPORT EQUATION

The relevant differential equations of interest here are similar in structure and can all be expressed by the following general equation for a variable $\emptyset$:

$$\partial(\bar{\rho}U_j\emptyset)/\partial x_j - \partial(\Gamma_\emptyset \partial\emptyset/\partial x_j)/\partial x_j = S_\emptyset \qquad (2.24\text{-}1)$$

where the expressions for the diffusivity $\Gamma_\emptyset$ and the source term $S_\emptyset$ can be deduced from the parent equations. The general equation (2.24-1) is made use of in the following chapter to simplify the development of the procedure for solving the equations. As a further preparatory step for the solution procedure, eq. 2.24-1 is re-expressed in cylindrical coordinates which are more suitable for the shape of the present solution domain. Hence, equation 2.24-1 becomes

$$1/r\ \partial[r(\rho V\phi - \Gamma\partial\phi/\partial r)]/\partial r + \partial(\rho U\phi - \Gamma\partial\phi/\partial x)/\partial x$$
$$+ 1/r\ \partial(\rho W\phi - \Gamma\partial\phi/r\partial\theta)/\partial\theta = S_\phi \qquad (2.24\text{-}2)$$

where S_ϕ = cylindrically transformed S_ϕ

+ additional terms due to the curvature effect after the coordinate transformation;

U, V, and W are the ensemble-averaged velocities in the axial, radial, and circumferential directions respectively. The averaging signs have been omitted for convenience.

Because of the large computer time and storage requirements, it is an expensive task to obtain solutions for multi-variables and three-dimensional fluid flow problems. Attention has been focussed in this thesis on axi-symmetrical problems in which $W = 0$ and $\partial/\partial\theta = 0$. However, the solution procedure developed here has the capability of straightforward extension to any non-symmetric or other 3-D problems. Equation 2.24-2 can thus be reduced as

$$1/r\ \partial[r(\rho V\phi - \Gamma\partial\phi/\partial r)]/\partial r + \partial(\rho U\phi - \Gamma\partial\phi/\partial x)/\partial x = S_\phi \qquad (2.24\text{-}3)$$

The expressions for Γ_ϕ and S_ϕ corresponding to the individual variable ϕ are listed in Table 2.24-1. These include the axial and radial velocities, the turbulent kinetic energy and its dissipation rate, and the stagnation enthalpy. Derivation of some of the source terms is shown in the following section.

The mass conservation equation 2.21-1 can also be expressed in cylindrical coordinates; for axi-symmetric steady flows that equation becomes:

$$1/r\ \partial(r\rho V)/\partial r + \partial(\rho U)/\partial x = 0 \qquad (2.24\text{-}4)$$

2.25 SOURCE TERMS FOR THE CONSERVATION EQUATIONS

a. Introductory Remarks

It can be established that for each conservation equation, there are three source terms due to the effects of the corresponding phase regions:

$$S_\phi = \begin{cases} S_l & \text{for} \quad 0 \le r \le r_l \\ S_m & \text{for} \quad r_l < r < r_{so} \\ S_{so} & \text{for} \quad r_{so} \le r \le R \end{cases} \qquad (2.25\text{-}1)$$

where r_l is the radius of the liquid-mushy interface, r_{so} of the solid-mushy interface and R of the mold. S_l represents the source term in the liquid region, S_m of the mushy and

S_{so} of the solid region. The expression of these terms are listed in Table 2.24-1. In these expressions, the formation of the buoyancy terms of the x-momentum equation in the liquid and mushy regions and the treatment of the latent heat term of the energy equation in the mushy region need special attention and is discussed in the following subsections.

b. Treatment of Buoyancy Terms in Liquid & Mushy Region

Liquid Region

In the present study, the body force is considered to be caused only by gravitational acceleration in a positive x direction. Thus, the formation of the buoyancy term via the axial pressure gradient and body force that appear in the x-momentum equation is

$$-\partial P/\partial x + \rho g \qquad (2.25\text{-}2)$$

If a reduced pressure P" is defined as

$$P'' = P - \rho_L\, g\, x \qquad (2.25\text{-}3)$$

where ρ_L is the fluid density at the liquidus line, which lies on the liquid-mushy interface (see, ref. [24]).

Differentiating the above pressure expression:

$$\partial P/\partial x = \partial P''/\partial x + \rho_L\, g \qquad (2.25\text{-}4)$$

Substituting the above expression in (2.25-2):

$$-\partial P^{*}/\partial x + g(\rho - \rho_L) \tag{2.25-5}$$

The density appearing in equation (2.25-2) can be related to the temperature via the Boussinesq model (see, ref. [9]), according to which density variations are considered only insofar as they contribute to buoyancy, but are otherwise neglected. Now, the thermal-expansion coefficient β for a fluid is defined as follows:

$$\beta = -(\partial\rho/\partial T)/\rho \tag{2.25-6}$$

For small density differences, this expression can be approximated:

$$(\rho - \rho_L) = -\beta\rho_L(T - T_L) \tag{2.25-7}$$

Then (2.25-2) becomes

$$\underset{\mathrm{I}}{-\partial P^{*}/\partial x} - \underset{\mathrm{II}}{g\beta\rho_L(T-T_L)} \tag{2.25-8}$$

where I = force due to the axial pressure gradient

II = buoyancy force due to natural convection

Mushy Region

The buoyancy terms in the x-momentum equation for the mushy region can be written as

$$-\partial P/\partial x + \rho_m g \tag{2.25-9}$$

where ρ_m is the density in the mushy region. By using the relation of (2.25-4), the expression (2.25-9) can be written as

$$-\underset{\mathrm{I}}{\partial P''/\partial x} + \underset{\mathrm{II}}{g(\rho_m - \rho_L)} \qquad (2.25\text{-}10)$$

where I = force due to the axial pressure gradient

II = buoyancy force due to natural convection

Following the treatment for the thermophysical properties in the mushy region, as described in subsection 2.41, the density can be defined as follows:

$$\rho_m = f_s\rho_S + (1-f_s)\rho_L \qquad (2.25\text{-}11)$$

where ρ_S is the density of solid at the solidus line which lies on the solid-mushy interface; and f_s is the solid fraction.

Substituting (2.25-11) into the expression (2.25-10), after rearrangement, the term becomes

$$-\partial P/\partial x + gf_s(\rho_S - \rho_L) \qquad (2.25\text{-}12)$$

It is seen that if f_s, ρ_L and ρ_S are known, the above terms can be calculated.

Next, in the following text, the superscript " is deleted from P" for convenience.

c. Treatment of Latent Heat in the Mushy Region

For pure substances, the latent heat of fusion is released at a unique temperature during phase change. However, for binary alloys, such as steel, the latent heat of fusion is released over a range of temperatures, namely between the liquidus[5] and solidus.[6]

By definition, the latent heat Q_L is equal to the product of the latent heat of fusion L_f and the rate of mass solidified $\dot{m}_{sol}$; i.e.,

$$Q_L = L_f \dot{m}_{sol} \qquad (2.25\text{-}13)$$

where $$\dot{m}_{sol} = [\partial(\rho U)/\partial x + 1/r\, \partial(r\rho V)/\partial r]_{sol} \qquad (2.25\text{-}14)$$

Based on the assumption of the homogenized flow in the mushy region, and also the treatment of thermophysical properties in the mushy region (see section 2.41b), it follows that

$$U_{sol} = U_m \quad \text{and} \quad V_{sol} = V_m \qquad (2.25\text{-}15)$$

$$\rho_{sol} = f_s \rho_s \qquad (2.25\text{-}16)$$

Hence, the resultant form of Q_L is

---

[5] Liquidus is the temperature at which the metal starts to solidify and the latent heat of fusion starts to release.

[6] Solidus is the temperature at which the metal is completely solidified and the latent heat of fusion has been completely released.

$$Q_L = L_f \rho_S [\partial(f_S U_m)/\partial x + 1/r\, \partial(r f_S V_m)/\partial r] \qquad (2.25\text{-}17)$$

Therefore, the assumption of a linear release of the whole latent heat (see, ref. [55, 7, 54]) is not always correct, as the combined effect of f_s and $(U_i)_m$ is not a simple function. It can be any function including linear, quadratic or exponential; and it should be treated as one of the solution's unknown parameters.

2.3 INTERFACE CONDITIONS

2.31 ADDITIONAL INTERFACE EQUATIONS

The four conservation equations, namely mass, energy, x-momentum and r-momentum, contain six basic unknowns. These include the velocity components U and V, the pressure P, the enthalpy H, the radius r_l of the liquidus interface and the radius r_{so} of the solidus interface. The interface radii shown in Fig. 2.31-1 vary with x and are used to derive two additional interface equations. The interface equations arise from the compatibility conditions and the energy balance, which are applied at all points along the solidus and liquidus interfaces (subsection 3.53).

2.32 COMPATIBILITY OF VELOCITIES AND TEMPERATURE

To simplify the problem formulation, no contact resistance between the casting and the mold is introduced even though consideration of it is possible. The liquidus interface is treated as a permeable boundary; i.e., liquid steel can flow into the mushy region.

From the above assumptions, no slip condition can be used; i.e., the tangential velocity components along the phase interfaces are the same. By mass continuity, the normal velocity components along the interfaces must also be the same.

At the solidus and liquidus lines, the values of temperatures at all points are the solidus and liquidus temperatures. Hence,

Solid-Mushy Interface

$$\phi_m = \phi_{so} = \phi_S \qquad (\phi = U,\ V,\ H,\ \text{etc.}) \qquad (2.32\text{-}1)$$

Liquid-Mushy Interface

$$\phi_m = \phi_l = \phi_L \qquad (\phi = U,\ V,\ H,\ \text{etc.}) \qquad (2.32\text{-}2)$$

where the subscripts m denotes the ϕ value next to the interface and also in the mushy region, l in the liquid, and so in the solid region. Subscripts S denotes the ϕ values at the solidus line, L at the liquidus line.

2.4 ADDITIONAL ALGEBRAIC EQUATIONS

Before the mathematical problem can be regarded as complete, it is necessary to formulate the additional algebraic equations, which include the boundary conditions of the problem, and the constituent equations which link various dependent variables together.

2.41 THERMOPHYSICAL PROPERTIES

a. Single Phase Region (Pure Liquid or Pure Solid)

Instead of the restrictive assumptions of constant conductivity K and constant pressure specific heat C_p of the materials in the single-phase liquid or solid region to obtain the solutions (see ref. [1,10,11,27,28]), the values of K and C_p are taken to be functions of temperature - a necessity in any realistic simulation of the heat flow in real materials over wide temperature ranges. So in a pure liquid or a pure solid region,

$$\not{Z}_a = \not{Z}_a(T) \qquad a = 1, so \qquad (2.41\text{-}1)$$

where $\not{Z}_m = K$ or C_p

In the present study, linear correlations between the temperature and these values in both regions are chosen for the following considerations:

(i) The computation of thermophysical properties must be made at every spatial grid point in the casting simulation. As this can involve millions of separate determinations of these properties during the execution of the computer program, there is a significant saving in the computing time by evaluating a linear relation instead of a more complicated form.

(ii) Definite trends are apparent in the data for steel and a series of linear segments adequately represents them.

To illustrate the foregoing ideas of using linear relations to approximate the values of C_p and K, low carbon steel is used (see ref. [29]). The conductivity K is represented by four linear segments as illustrated in Fig. 2.41-1. It is given, in general form, as

$$K = K1 - K2(T - K3) \qquad (2.41\text{-}2)$$

where K1, K2 and K3 are different constants defined in Table 2.41-1 to specify each segment. Selected data and functional relationships for the specific heat are illustrated in Fig. 2.41-2. In general, the specific heat C_p can be expressed as

$$C_p = C1 + C2(T - C3) \qquad (2.41\text{-}3)$$

where C1, C2 and C3 are different constants defined in Table 2.41-2 to specify each segment.

In most practical applications, density and viscosity can be assumed to be constant without any significant errors in the prediction (see ref. [29]). In the present study, these constant values are listed in Table 4.11-1.

b. Mushy Region

I. OVERALL TREATMENT

The thermophysical properties in the two-phase mushy region need special attention, since they do not only depend on the temperature, as in the single-phase liquid or solid region, but they depend also on the two-phase effect in this region. The following are assumed;

(i) The solid fraction can be analogous to the thermodynamic property of the quality in relation to the intensive properties (see ref [39]).

(ii) All the thermophysical properties such as density, conductivity and viscosity, are functions of temperature (see ref. [50]).

(iii) A linear relationship exists between the solid fraction and the temperature (see ref. [30]).

(iV) Homogenized transport has been assumed in the mushy region.

Because of the above considerations, a general expression for g_m in the mushy region can be defined as follows:

$$g_m(f_s, T) = f_s g_S + (1 - f_s) g_L \qquad (2.41\text{-}4)$$

where g_m represents the thermophysical in the mushy region, g_L at the liquidus line, and g_S at the solidus line. The solid fraction f_s, which reflects the presence of the two phases, is defined in the following subsection.

II. SOLID FRACTION

The solid fraction f_s in the mushy region can be defined as follows:

$$f_s = m_{so}/(m_{so} + m_l) \qquad (2.41\text{-}5)$$

where m_{so} is the local mass of solid, and m_l of liquid. As m_{so} and m_l are difficult to determine analytically, unless additional mass conservation equations are solved, their values are usually approximated and expressed as a function of known quantities.

The following relations are assumed.

$$f_s = \begin{cases} 0, & T_L \leq T \\ f_s(T), & T_S < T < T_L \\ 1, & T < T_S \end{cases} \qquad (2.41\text{-}6)$$

The relationship between the solid fraction and the temperature can be supported on the basis of the phase diagram. In the present work, a linear relationship between the solid fraction and the temperature in the mushy zone is assumed. This corresponds to the simple case presented by Miyazawa and Muchi [39]. Therefore,

$$f_s = (T_L - T)/(T_L - T_S) \qquad (2.41\text{-}7)$$

2.42 BOUNDARY CONDITIONS

a. General Requirements

The flows examined in this study are of an elliptic[7] nature; it is necessary to supply the conditions for all the variables at the boundaries of the solution domain. These conditions are usually specified as:

(i) the value of the dependent variable at the boundaries,
(ii) the value of the associated flux, and
(iii) a relation between the two.

---

[7] Elliptic flows are those where perturbations of conditions at any point in the flow can influence conditions at any other point. Such flows are governed by partial differential equations of the type known as "elliptic" - such as those given by eq.2.24-1 (see ref. [13]).

Since velocities and pressure are inter-dependent, either the velocities or the pressures need to be prescribed.

The general conditions at the various boundaries are discussed in the following subsections.

b. Special Surface Boundaries for Energy Equation

I. GENERAL TREATMENT

At the surface boundary, two cases of boundary conditions are considered:

Dirichlet Boundary

The boundary surface temperature is known or given in the study.

Neumann Derivative Boundary

In this case, the boundary surface temperature is not known and the boundary condition is given as normal temperature gradient. This may be conductive, convective, radiative, or the combination of them.

For convective boundary conditions, the normal energy transfer can be written as

$$\partial H/\partial n = - h(T_b - T_a) \qquad (2.42\text{-}1)$$

where h = heat transfer coefficient

T_b = the boundary temperature

T_a = the ambient temperature

For radiative boundary conditions, the normal energy transfer may be written as

$$\partial H/\partial n = \sigma EF(T_b{}^4 - T_a{}^4) \qquad (2.42\text{-}2)$$

where σ is the Stefan-Boltzmann constant, E is emissivity, and F is the view factor.

The cooling of the metal in the continuous casting process is discussed in the following subsections and is illustrated in Fig. 2.42-1.

II. MOLD COOLING

The region of mold cooling starts from the top of the mold and ends at x_{mold} (see Fig. 2.42-1). In the mold, the metal and mold are initially in good thermal contact and heat transfer is by conduction. As the metal solidifies downward, it contracts and breaks away from the mold. Eventually, an air-gap is formed between the solidified shell and the mold, and heat transfer is by radiation and convection. Taking into account the time of gap formation and its size, Savage and Pritchard [43] proposed a heat flux expression over the complete length of the mold;

$$Q_{mold} = A - B(t^{1/2}) \qquad (2.42\text{-}3)$$

where A and B are constants determined through experiments, t is time where time is equal to:

$$t = x_{mold}/U \tag{2.42-4}$$

III. WATER SPRAY COOLING

The water spray cooling starts from the end of the mold and ends at x_{spray} (see Fig. 2.42-1). In this region the heat transfer mechanism is complex (nucleate boiling and forced convection). In the present study, convective heat transfer is assumed to be dominant (see ref. [31]) and its expression is given by the relation (2.42-1), where h is now the average heat transfer coefficient for the spray-cooled region, and T_a is the spray water temperature.

IV. AIR RADIATION COOLING

The region of air radiation cooling continues the region of spray cooling until complete solidification has occured. The heat transfer is mainly due to radiation, and is given by the relation (2.42-2).

c:- Other Boundaries

I. WALLS

Since the mold wall is at rest, the velocity must be zero at all points on its surface. The exterior boundary of the shell of the solidified metal, can be treated as a moving wall with only axial velocity componeht; therefore, the radial velocity and the radial flux are zero.

$$U = V = k = \epsilon = 0 \quad \text{at mold wall}$$

$$V = \partial \phi / \partial r = 0 \quad \text{at the moving wall (solid shell)} \qquad (2.42\text{-}5)$$

where $\phi = k$ and ϵ .

II. INLET/OUTLET APERTURES

The computational domain is shown in Fig. 4.22-2. At the inlet (nozzle exit), the velocities and enthalpy are imposed and considered to be uniform. At the exit of the system (withdrawal of the solid steel), zero gradients of ϕ are assumed. Hence,

$$\phi = \phi_{imposed} \quad \text{at the inlet nozzle}$$

$$(\partial \phi / \partial x)_1 = 0 \quad \text{at the outlet} \qquad (2.42\text{-}6)$$

where $\emptyset$ = U, V, H, k and ϵ

Using the mass conservation equation, an additional constraint can be found:

$$\Sigma \dot{m}_{in} = \Sigma \dot{m}_{out} \quad (2.42\text{-}7)$$

and from this, the following expression can be obtained,

$$\Sigma (\rho U)_1 A_{noz} = \Sigma (\rho U)_{so} A_{mo} \quad (2.42\text{-}8)$$

where $\dot{m}_{in}$ is the rate of total mass in, and $\dot{m}_{out}$ of the total mass out of the solution domain. A_{noz} is the cross-sectional area of the inlet nozzle, and A_{mo} of the outlet solidified metal.

III. SYMMETRY AXIS

On the symmetry axis the gradient of all the variables with respect to r must be zero because of the symmetry. The radial velocity must also be zero to avoid a velocity discontinuity. Hence,

$$V = \partial\emptyset/\partial x = 0. \quad (2.42\text{-}9)$$

where $\emptyset$ = U, H, k and ϵ

IV. FREE SURFACE

There is a free surface of liquid steel at the top of the mold. In practice, free slip condition is applied at the free surface; therefore, the gradient of radial velocity with respect to x axis, and the axial velocity must be zero. If the free surface is assumed to adiabatic, the temperature gradient with respect to x axis is zero. Hence,

$$U = \partial Ø/\partial x = 0 \qquad (2.42\text{-}10)$$

where $Ø$ = V, H, k and ϵ

2.5 CLOSURE

The mathematical formulation of the problem has been presented. It can be summarized as follows:

(i) The basic governing transport equations of heat, mass, and momentum have been presented in ensemble-averaged form.

(ii) The essential features of the k-ϵ turbulent viscosity model adopted in this simulation have been given.

(iii) The complete set of equations for both mean flow variables and turbulence quantities have been presented in the form that they are to be solved, and the resulting general transport equation has been given.

(iv) Four conservation equations and two additional equations arising from the compatibility conditions and the energy balance along the interface lines have also been identified.

(v) The boundary conditions required for the solution of the equations have been shown.

(vi) The thermophysical and the two-phase properties have also been presented.

Differential equations are discretized to obtain a set of algebraic equations. The method used is presented in the following chapter.

CHAPTER 3

THE SOLUTION PROCEDURE

3.1 INTRODUCTION

This chapter is concerned with the development of a numerical procedure for solving the set of elliptic, partial-differential equations, obtained in Chapter 2. In section 3.2 the differential equations are converted into a form suitable for numerical solution by using the 'finite-volume method' approach in which the discretized form of equations is obtained by integration of the differential equations over finite volumes of 'cells'. After the expressions for the flux and source terms are obtained, the discretized equations are assembled.

The determination of the local thermophysical properties at the control volume boundary, and for the whole control volume, is discussed in section 3.3.

The SIMPLE algorithm with the line-by-line iteration method is used for solving the equations of motion, as outlined in subsection 3.41. Novel algorithms for the energy equation and the interface searching procedures for the solidus and liquidus lines are presented in the following two subsections. Some aspects of the convergence and numerical stability are discussed in the last section.

3.2 DERIVATION OF DISCRETIZED EQUATIONS

The transport equations of relevance are too complex to be solved analytically; hence, a numerical solution is required. One of the most widely used numerical methods for fluid problem is the 'finite-volume method' (see ref. [12,13,15]), in which the calculation domain is divided into a finite number of discrete volumes or 'cells' by a computational grid, and numerical values of the dependent variables are determined at the centre of the cells.

3.21 GRID AND NOTATION

Based on the 'finite-volume method' approach, the numerical solution consists of subdividing the domain into a series of non-overlapping and continuous discrete control volumes or cells. Using the staggered grid arrangement [44], all scalar quantities, such as enthalpy and pressure are calculated at the nodal points of the grid, while the velocities are calculated at cell boundaries. The velocities, which are designated by the arrows in the diagram as shown in Fig. 3.21-1, are displaced so as to lie midway between the grid points. This positioning has the advantage that the velocities lie on the boundaries of the 'finite volume' cells for scalar dependent variables. Thus they are directly available for calculating convection through these walls.

Figure 3.21-1 shows a typical node P, its nearest neighbours labelled, N, E, S, and W, and the intervening cell boundaries, labelled, n, e, s and w. For cylindrical coordinates the cells are formed by rotating the grid through a unit angle around the symmetry axis of the centre line. The advantages of the staggered grid are as follows:

(i) The pressure gradient is directly available for the calculation in the momentum equations.

(ii) The discretized continuity equations are based on the differences of adjacent velocity components. This eliminates the possibility of getting an unrealistic wavy velocity field (see comments by Patankar [36]).

In the following subsections, the subscripts (l,ξ), (m,ξ) and (so,ξ) denote respectively the mean quantities of liquid, mushy and solid regions at the ξ boundary of the control volume. For example, $Q_{l,e}$ denotes the mean transport of liquid region at the e (east) boundary as shown in Fig. 3.21-2. The subscripts L and S represent the quantities at the liquidus and solidus lines respectively.

3.22 INTEGRATION OF THE GENERAL DIFFERENTIAL EQUATION

The integral form of the general transport equation 3.24-3 over the control volume centered at P and shown in Fig. 3.21-1, is written as

$$\iint_V \left\{\frac{1}{r}\frac{\partial}{\partial r}\left[r\left(\rho V\phi - \Gamma\frac{\partial \phi}{\partial r}\right)\right] + \frac{\partial}{\partial x}\left(\rho U\phi - \Gamma\frac{\partial \phi}{\partial x}\right)\right\}dV = \iint_V S_\phi \, dV \qquad [3.22\text{-}1]$$

where V is the volume of the control volume.

By the divergence theorem, the equation may be rewritten as,

$$\underbrace{(Q_e - Q_w + Q_n - Q_s)}_{\text{total transport across the cell boundaries}} = \underbrace{\int_{r_s}^{r_n}\int_{x_w}^{x_e} S_\phi \, r\,dr\,dx}_{\text{source generation or dissipation}} \qquad [3.22\text{-}2]$$

where Q_e, Q_w, Q_n, and Q_s are the total transport of ϕ, due to convection and diffusion, across the east, west, north, and south boundaries of the control volume, and are defined as,

$$Q_e = \int_{r_s}^{r_n} \left[\rho U\phi - \Gamma\frac{\partial \phi}{\partial x}\right]_{x_e} r\,dr \quad , \qquad [3.22\text{-}3]$$

$$\text{and} \quad Q_n = \int_{x_w}^{x_e} [\rho v \phi - \Gamma \frac{\partial \phi}{\partial r}]_{r_n} r_n dx \quad . \qquad [3.22\text{-}4]$$

3.23 DISCRETIZATION OF THE INTEGRATED EQUATION

a. Expression for the Flux Terms

The law of conservation requires that total transport of any quantity across any boundary of a multi-region control volume is equal to the summation of all the total transports generated from each phase region across the same boundary. Thus the total transport Q on any (east, west, north or south) boundary may be rewritten generally as

$$Q = \sum Q_{\xi} \qquad [3.23\text{-}1]$$

where $\sum$ denotes the summation of the total transport contributed by all phases ξ involved. In the present study three regions, namely the liquid, mushy and solid regions (i.e. ξ = l, m or so), are considered. Thus, there are four different cases for expressing the transport terms for each boundary of the control volume as illustrated in Fig. 3.22-1 and Fig. 3.22-2.

The expressions for the total transport at any boundary, which can be applied to each case, can be compactly written as

$$Q_i = \int_{r_s}^{I_{1,i}} q_i \, r dr + \int_{I_{1,i}}^{I_{2,i}} q_i \, r dr + \int_{I_{2,i}}^{r_n} q_i \, r dr, \qquad i = e \text{ or } w \tag{3.23-2a}$$

(see, for example, the east boundary of the control volume in Fig. 3.23-1.)

$$Q_j = \int_{x_w}^{I_{1,j}} q_j \, r_j dx + \int_{I_{1,j}}^{I_{2,j}} q_j \, r_j dx + \int_{I_{2,j}}^{x_e} q_j \, r_j dx, \quad j = n \text{ or } s \tag{3.23-2b}$$

(see, for example, the north boundary of the control volume in Fig.3.23-1.)

where Q_is denotes the total transports in axial direction, and Q_j in radial direction. (see Fig. 3.22-2 for illustration of Q_e and Q_n). q denotes the total flux which is the sum of the convection flux and the diffusion flux. Thus,

$$q_i = [\rho U\phi - \Gamma \frac{\partial\phi}{\partial x}]_i \quad , \tag{3.23-3a}$$

$$q_j = [\rho V\phi - \Gamma \frac{\partial\phi}{\partial r}]_j \quad . \tag{3.23-3b}$$

$I_{1,i}$ and $I_{2,i}$, are the axial integration limits. $I_{1,j}$ and $I_{2,j}$ are the radial integration limits. These limits can be used to classify the four different cases.

Before these cases are shown, certain integration limits have to be defined for later clarification: $I_{L,i}$ (i = e, w) is the radial limit of the liquidus line and $I_{S,i}$ of the solidus lines at the corresponding boundary, measured radially from the axis of the cylindrical co-ordinate system, as shown in Fig. 3.22-1. Similar limits can be defined in the axial direction; and they are $I_{L,j}$ and $I_{S,j}$ (j = n, s).

The four cases are shown in Fig. 3.22-1 and presented in the following relations:

(1) $I_1 = I_L$ and $I_2 = I_S$

Both liquidus and solidus lines intercept the boundary, i.e., all three phases, liquid, mushy, and solid, occupy the boundary. (see, for example, the east boundary of the control volume)

(2) $I_1 = I_2 = I_S$

Only the solidus line intercepts the boundary, i.e. solid and mushy regions occupy the boundary. (see, for example, the north boundary of the control volume)

(3) $I_1 = I_2 = I_L$

Only the liquidus line intercepts the boundary, i.e. liquid and mushy regions occupy the boundary. (see, for example, the west boundary of the control volume)

(4) $\underline{I_1 = I_2}$

Neither liquidus nor solidus lines intercept the boundary, i.e. only the single phase such as liquid, mushy or solid occupies the boundary. (see, for example, the south boundary of the control volume)

The first case, which is the most general one, is used to illustrate the discretization of the total transport terms. Similar treatment can be applied to other cases at all the boundaries with the adjustments of the corresponding integration limits. By using the mean-value theorem, we can assume the fluxes for each region to be constant along every cell boundary. Thus the above integrals from expressions (3.23-2) may be replaced as

$$Q_i = \Sigma [\bar{q} A]_{\xi,i} \quad , \qquad [3.23-4a]$$

$$Q_j = \Sigma [\bar{q} A]_{\xi,j} \quad . \qquad [3.23-4b]$$

where $A_{\xi,i}$ is the area occupied by the ξ region on the i boundary, and $A_{\xi,j}$ on the j boundary. Their expressions will be given later. The superbar ($^-$) represents the mean value of the variables and will be dropped from now on for the simplicity of notation.

To relate all the unknown $A_{\xi,i}$ (or $A_{\xi,j}$) to the known total area of the i (or j) boundary, to simplify the algebraic expression of the equations which has the same form as the usual single phase problem, and to simplify the searching procedure for the interfaces as shown later in subsection 3.42, the dimensionless area ratio $\gamma_{\varrho,i}$ of the ϱ region on the i boundary, and $\gamma_{\varrho,j}$ on the j boundary are introduced and defined as

$$\gamma_{\varrho,i} = A_{\varrho,i}/A_i \quad \text{and} \quad \gamma_{\varrho,j} = A_{\varrho,j}/A_j \qquad [3.23\text{-}5]$$

where A_i is the total area of i boundary, and A_j of j boundaries. From the above γ definitions, the following expressions result:

$$\sum \gamma_{\varrho,i} = 1 \quad \text{and} \quad \sum \gamma_{\varrho,j} = 1 \quad . \qquad [3.23\text{-}6]$$

For the above mentioned phase regions at the boundaries, the expressions of γ can be written as

<u>Axial Dimensionless area ratio</u> $\gamma_{\varrho,i}$

$$\gamma_{1,i} = \frac{I_{1,i}{}^2 - r_s{}^2}{A_i} \quad , \quad \gamma_{so,i} = \frac{r_n{}^2 - I_{2,i}{}^2}{A_i} \quad ,$$

$$\gamma_{m,i} = 1 - \gamma_{1,i} - \gamma_{so,i} \quad . \qquad [3.23\text{-}7]$$

where $A_i = r_J \Delta r_J$. (see, for example, the east boundary of the control volume in Fig. 3.23-2)

<u>Radial Dimensionless area ratio</u> $\gamma_{\varrho,j}$

$$\gamma_{1,j} = \frac{r_j(I_{1,j} - x_w)}{A_j} \quad ; \quad \gamma_{so,j} = \frac{r_j(x_e - I_{2,j})}{A_j} \quad ,$$

$$Y_{m,j} = 1 - Y_{1,j} - Y_{so,j} \quad . \qquad [3.23\text{-}8]$$

where $A_j = r_j \Delta x_I$. (see, for example, the north boundary of the control volume in Fig. 3.23-3)

Making uses of above definition, Qs from expression (3.23-4) becomes

$$Q_i = q_i^{eff} A_i \quad \text{and} \quad Q_j = q_j^{eff} A_j \qquad [3.23\text{-}9]$$

where $q_i^{eff} = \sum [q\ Y]_{g,i}$ and $q_j^{eff} = \sum [q\ Y]_{g,j}$.

Using the definition of q from Eq. (3.23-3), the $[qY]$ can be written as

$$[qY]_i = (\rho U Y)\phi - (\Gamma Y)\frac{\partial\phi}{\partial x} \quad \text{and} \quad [qY]_j = (\rho U Y)\phi - (\Gamma Y)\frac{\partial\phi}{\partial r} \qquad [3.23\text{-}10]$$

Therefore, q^{eff} can be rewritten as

$$q_i^{eff} = [C^{eff}\ \phi - (\delta x_i D^{eff})\frac{\partial\phi}{\partial x}]_i \qquad [3.23\text{-}11a]$$

$$q_j^{eff} = [C^{eff}\ \phi - (\delta r_j D^{eff})\frac{\partial\phi}{\partial r}]_j \qquad [3.23\text{-}11b]$$

where C_i^{eff} (or C_j^{eff}) is the effective convection coefficient on the i (or j) boundary, and D_i^{eff} (or D_j^{eff}) is the effective diffusive coefficient on the i (or j) boundary. They are defined as

$$C_i^{eff} = \sum [(\rho U Y)_g]_i \quad , \quad C_j^{eff} = \sum [(\rho V Y)_g]_j \qquad [3.23\text{-}12]$$

$$D_i^{eff} = \sum [(\Gamma Y)_\varsigma/\delta x]_i \quad , \quad D_j^{eff} = [(\Gamma Y)_\varsigma/\delta r]_j \qquad [3.23-13]$$

For simplicity the superscript 'eff' for the flux terms will be dropped from now on. Approximate expression of boundaries $\emptyset$ and $(\partial\emptyset/\partial x)$ in terms of nodal values of $\emptyset$ is presented in subsection 3.24.

b. Expression for the Source Terms

The conservation law requires that the total source term within a multiphase control volume should be equal to the summation of all the source terms contributed by the phase regions involved. Therefore, the total source terms $\bar{S}$ can be generally written as

$$\bar{S} = \iint_V S_\emptyset \, dV = \iint_{V_\varsigma} S_{\emptyset,\varsigma} \, dV \qquad [3.23-14]$$

(Compare this expression with the general flux expression (3.2-1).)

where ς for the present problem, can be equal to l, m, or so, depending upon the regions involved. Using the mean-value theorem; i.e. assuming mean values of $S_\emptyset$ in the region of interest, the total source term $\bar{S}$ can be rewritten as

$$\bar{S} = \sum [\bar{S}_\emptyset \delta V]_\varsigma \qquad [3.23-15]$$

where $\bar{S}_{\phi,\xi}$ is the mean value of S_ϕ of the ξ region; and δV_ξ is the volume occupied by the ξ region of a multiphase control volume.

Following the practice as before, the dimensionless volume ratios are introduced and thus we have

$$\theta_\xi = \delta V_\xi / \delta V \qquad [3.23\text{-}16a]$$

$$\sum \theta_\xi = 1 \qquad [3.23\text{-}16b]$$

where θ_ξ is the dimensionless volume ratio of ξ region; and δV is the total volume of the control volume.

Making use of the definition of θ, the total source term $\bar{S}$ from expression (3.23-15) becomes

$$\bar{S} = S^{eff}\ \delta V \qquad [3.23\text{-}17]$$

where S^{eff} is the effective source term for the multi-region control volume and is defined as

$$S^{eff} = \sum [\bar{S}_\phi \theta]_\xi \qquad [3.23\text{-}18]$$

Approximate expression of $\bar{S}_\phi$ for different transport quantities will be presented in the later section. For notation simplicity the superbar ($^{-}$) will be omitted from now on. The evaluation of θs are now given.

In the present problem there are four possible types of control volume. In each type of control volume, there are different cases because the involved phase regions have various geometrical shapes, as shown in Fig. 3.23-4. They are classified as follows:

(1) <u>Single Region Control Volume</u>

Neither liquidus nor solidus lines intercept the control volume; i.e., only θ_l or θ_m or $\theta_{so} = 1$. Thus three corresponding cases are possible.

(2) <u>Liquid-Mushy Region Control Volume</u>

Only the liquidus line intercepts the control volume; i.e., $\theta_{so} = 0$, $\theta_l \neq 0$ and $\theta_m \neq 0$. Thus six corresponding cases are possible.

(3) <u>Solid-Mushy Region Control Volume</u>

Only the solidus line intercepts the control volume; i.e., $\theta_l = 0$, $\theta_m \neq 0$ and $\theta_{so} \neq 0$. Thus six corresponding cases are possible.

(4) <u>Liquid-Mushy-Solid Region Control Volume</u>

Both liquidus and solidus lines intercept the control control volume; i.e., $\theta_l \neq 0$, $\theta_m \neq 0$ and $\theta_{so} \neq 0$. Thus fourteen corresponding cases are possible.

Using the condition (3.23-16b) the dimensionless volume ratio θ_m can be calculated by

$$\theta_m = 1 - \theta_l - \theta_{so} \qquad [3.23\text{-}19]$$

The expressions of θ_l and θ_{so} (which are related to the dimensionless area ratio γ) are described for the four types of control volume by the following two generalized expressions (see Appendix 1 for detailed derivation).

$$\theta_{\xi} = 1 - \tfrac{1}{2}\{(1 - \gamma_e)[(1 - \gamma_n) + (1 - \gamma_s)] + (1 - \gamma_w)[(1 - \gamma_n) + (1 - \gamma_s)]\}_{\xi} \qquad [3.23\text{-}21]$$

$$\theta_{\xi} = [\tfrac{1}{2}(\gamma_e + \gamma_w)(\gamma_n + \gamma_s)]_{\xi} \qquad [3.23\text{-}20]$$

The conditions for using the above equations, which are subjected to different values of γ, are as follows:

(i) <u>All $\gamma_{l,k} = \gamma_{so,k} = 0$</u> where $k = e, w, n$ or s

$$\theta_l = \theta_{so} = 0 \qquad [3.23\text{-}22]$$

(ii) <u>All $\gamma_{l,k} \neq 0$</u>

$$\theta_l = \text{Exp. } (3.23\text{-}21) \qquad [3.23\text{-}23]$$

$$\theta_{so} = \text{Exp. } (3.23\text{-}20)$$

(iii) <u>All $\gamma_{so,k} \neq 0$</u>

$$\theta_{so} = \text{Exp. } (3.23\text{-}21) \qquad [3.23\text{-}24]$$

$$\theta_l = \text{Exp. } (3.23\text{-}20)$$

(iv) <u>Not all $\gamma_{\xi,k} \neq 0$</u>

$$\theta_{\xi} = \text{Exp. } (3.23\text{-}20) \qquad [3.23\text{-}25]$$

3.24 FLUX DISCRETIZATION

The hybrid difference scheme (Spalding [45]), which blends the advantages of central and upwind difference schemes, is used to discretize the expression $\emptyset$ at all cell boundaries.

The hybrid difference scheme applied for the east boundary of the control volume in Fig. 3.21-1 is,

$$Q_e = \begin{cases} C_e \emptyset_E & \text{for } Pe_e < -2 , \\ \frac{1}{2} C_e(\emptyset_E + \emptyset_P) - D_e(\emptyset_E - \emptyset_P) & \text{for } |Pe_e| \leq 2 , \\ C_e \emptyset_P & \text{for } Pe_e > 2 . \end{cases} \qquad [3.24\text{-}1]$$

where Pe_e is a Peclet number for the east boundary and defined by $Pe_e = C_e/D_e$. Pe is actually the ratio of convection to diffusion. Similar expressions can be written for all the other cell boundaries.

3.25 ASSEMBLY OF DISCRETIZED EQUATIONS

Substituting the discretized flux terms and source terms from section 3.23a and 3.23b respectively into the general differential equation (3.22-2), the final discretization equation for the hybrid scheme can now be written as

$$a_P \emptyset_P = a_E + a_W \emptyset_W + a_N \emptyset_N + a_S \emptyset_S + b , \qquad [3.25\text{-}1]$$

where $a_E = \max[-C_e, D_e-(C_e/2), 0]$

$$a_W = \max[C_w, D_w+(C_w/2), 0]$$

$$a_N = \max[-C_n, D_n-(C_n/2), 0]$$

$$a_S = \max[C_s, D_s+(C_s/2), 0]$$

$$a_P = a_E + a_W + a_N + a_S$$

$$b = \underline{S}_{eff}\ \delta V$$

$$a_P = a_E + a_W + a_N + a_S$$

3.3 DETERMINATION OF LOCAL THERMOPHYSICAL PROPERTIES

The determination of the local thermophysical properties at the control volume boundary and for the whole control volume are presented in this section.

3.31 PRELIMINARY REMARKS

The thermophysical properties Ξ (k, Cp, ρ, μ) of the single-phase region, such as the liquid or solid region, are given either as constants or as known functions (see section 3.41). Hence, more attention will be focussed on the determination of local thermophysical properties in the mushy region as they usually vary between the values at the liquidus line and the values at the solidus line.

Two categories of 'local' properties have been computed for the mushy region, namely the property computed at the boundary of the control volume and the property computed for the whole control volume. The first category is used in the computation of the convective and diffusive terms, whereas the second category is used in the computation of the body-force terms. The computation is carried out for the four kinds of control volume (see Fig. 3.23-1).

3.32 PROPERTIES AT THE CONTROL VOLUME BOUNDARY

In general the mean properties $\bar{\varnothing}_m$ at the control volume boundary of the mushy region can be calculated by

$$\bar{\varnothing}_{m,i} = \frac{1}{A_{m,i}} \int_m \varnothing_m \, r \, dr \qquad , \qquad i = e, w \qquad [3.32\text{-}1a]$$

$$\bar{\varnothing}_{m,j} = \frac{1}{A_{m,j}} \int_m \varnothing_m \, r_j \, dx \qquad , \qquad j = n, s \qquad [3.32\text{-}1b]$$

where $A_{m,i}$ is the boundary area occupied by the mushy region at the i boundary, and $A_{m,j}$ at the j boundary. The integration is carried out within the mushy region.

Substituting the expression of $\varnothing_m$ from Eq (3.41-4) (which is in linear form of mass fraction) into the above equations, yields:

$$\bar{Z}_{m,i} = Z_L + \frac{1}{A_{m,i}} \int_m f_s \, r dr \, (Z_S - Z_L) \qquad [3.32\text{-}2a]$$

$$\bar{Z}_{m,j} = Z_L + \frac{1}{A_{m,j}} \int_m f_s \, r_j dx \, (Z_S - Z_L) \qquad [3.32\text{-}2b]$$

Making use of the mean value theorem, we can rewrite the above equations as

$$\bar{Z}_{m,\xi} = Z_L + [\bar{f}_s]_\xi (Z_S - Z_L) \qquad [3.32\text{-}3]$$

where $[\bar{f}_s]_\xi$ is the mean mass fraction at the mushy boundary of the control volume.

Based on the previous assumption that a linear relationship exists between the solid fraction and the temperature in the mushy region (see section 3.41b) and Eq. (3.41-7), $[\bar{f}_s]_\xi$ can be approximated as (see ref. [30]):

$$[\bar{f}_s]_\xi = \frac{1}{T_S - T_L} (\bar{T}_{m,\xi} - T_L) \quad , \quad \xi = i,\ j. \qquad [3.32\text{-}4]$$

where $\bar{T}_{m,\xi}$ is the mean temperature of the mushy region at the ξ boundary. How it is determined is discussed in this chapter.

Equations (3.32-3 and 3.32-4) show that $\bar{Z}_m$ is a direct function of temperature; i.e., $\bar{Z}_m = \bar{Z}_m(T)$; hence, attention is focussed on the method for determining the mean temperature $T_{m,\xi}$. The east boundary of a typical P-centre control volume is used as an illustration (see Fig. 3.32-1). In the present studies the dimensionless area ratio γ's, nodal temperatures T_P and T_E, liquidus temperature T_L, and solidus temperature T_S are the chosen parameters in the formulation of the approximation of $T_{m,\xi}$. The approximation of $T_{m,\xi}$ is given as follows:

(i) $\underline{\text{All } \gamma_{\varrho,e} \neq 0}$ where ϱ = 1, m, or so

Since both liquidus and solidus lines intercept the east boundary (Fig. 3.32-1a), the mean temperature at the east mushy boundary is approximated as

$$T_{m,e} = \frac{1}{2} (T_L + T_S) \qquad [3.32\text{-}5]$$

(ii) $\underline{T_L > (T_P, T_E) > T_S}$

Both centre and east nodal temperatures lie in the mushy region (Fig. 3.32-1b). If the temperature is assumed to vary linearly in the east direction,

$$T_{m,e} = \frac{1}{2} (T_P + T_E) \qquad [3.32\text{-}6]$$

(iii) $\underline{\gamma_{m,e} \neq 1}$

(a) $\underline{T_P, T_E < T_S}$ or $\underline{T_P > T_S > T_E}$

Where both centre and east nodal temperatures lie in the solid region; and also where only the centre nodal temperature lies in the mushy region while the east nodal temperature lies in the solid region (see Fig. 3.32-1c), the mean temperature at the east mushy boundary is approximated as

$$T_{m,e} = T_S \qquad [3.32\text{-}7]$$

(b) $\underline{T_P,\ T_E > T_L}$ or $\underline{T_P > T_L > T_E}$

Where both centre and east nodal temperatures lie in the liquid region; and for the case where only the east nodal temperature lies in the mushy region, while the centre nodal temperature lies in the liquid region (see Fig. 3.32-1d), the mean temperature at the east mushy boundary is approximated as

$$T_{m,e} = T_L \qquad [3.32\text{-}8]$$

3.33 PROPERTIES FOR THE WHOLE CONTROL VOLUME

In general, properties $\bar{\phi}$ for the whole control volume of the mushy region can be defined as

$$\bar{\phi} = \frac{1}{V_m} \int_m \phi \, dV \qquad [3.33\text{-}1]$$

where V_m is the control volume occupied by the mushy region.

Following the same derivations as those presented in the subsection 3.32, the mean mass fraction $\bar{f}_s$ for the whole control volume can be expressed as (c.f. Eq. 3.32-4)

$$\bar{f}_s = \frac{1}{T_S - T_L} (\bar{T}_m - T_L) \qquad [3.33-2]$$

where $\bar{T}_m$ is the mean temperature of the mushy region for the whole control volume. A typical P-centre control volume is used as an illustration, as shown in Fig. 3.33-1. T_P, T_L, and T_S are the chosen parameters in the formulation of the approximation of $\bar{T}_m$, which is given as

(i) $\underline{T_L > T_P > T_S}$

The nodal temperature lies in the mushy region, as shown in Fig. 3.33-1a. In this case the nodal temperature is assumed to prevail uniformly within the mushy region,

$$\bar{T}_m = T_P \qquad [3.33-1]$$

(ii) $\underline{\text{All } \theta_g \neq 0}$ and $(\underline{T_P > T_L}$ or $\underline{T_P < T_S})$

Both liquidus and solidus lines intercept the control volume, and the nodal temperature lies outside the mushy region, as shown in Fig. 3.33-1b. The mean temperature for the whole mushy region is approximated as

$$\bar{T}_m = \frac{1}{2} (T_L + T_S) \qquad [3.33-2]$$

(iii) $\underline{\theta_m \neq 0}$ and $(\underline{\theta_l \neq 0}$ or $\underline{\theta_{so} \neq 0})$

(a) $\underline{T_p > T_L}$

Only the liquidus line intercepts the control volume, and the nodal temperature lies in the liquid region, as shown in Fig. 3.33-1c. The mean temperature for the whole mushy region is approximated as

$$\bar{T}_m = T_L \qquad [3.33-3]$$

(b) $\underline{T_p < T_S}$

Only the solidus line intercepts the control volume, and the nodal temperature lies in the solid region, as shown in Fig. 3.33-1d. The mean temperature for the whole mushy region is approximated as

$$\bar{T}_m = T_S \qquad [3.33-4]$$

3.4 GENERAL SOLUTION ALGORITHM

Different algorithms have been developed to solve the equations of motion, the energy equation, the interface lines tracing procedure, and the overall procedure. The algorithms are presented in the following subsections.

3.41 EQUATIONS OF MOTION

a. The Solution of Discretized Equations

For M differential equations, there are N×M algebraic ones to be solved, where N is the number of grid nodes.

1) Preliminary Consideration

The discretized equations are cast into a linear form, but no particular method is assumed for their solution. Therefore, any suitable solution method can be employed at this stage.

Direct methods (i.e., those require no iteration, but require rather large computer storage and time) are not economical for nonlinear problems, since the equations have to be solved repeatedly with updated coefficients. Therefore, the alternatives are iterative methods, which start from a guessed field of the dependent variable; e.g.,U and V and use algebraic equations to obtain an improved field until convergence conditions have been satisfied. Iterative methods, unlike direct methods, usually require very small additional computer storage; therefore, they are especially attractive for solving coupled nonlinear equations. This study uses iterative methods to solve such equations.

There are many iterative methods for solving algebraic equations. A line-by-line iterative method is used and discussed in the following subsection.

2) The Line-by-Line Iterative Method

A line-by-line iterative method is a convenient combination of the direct method (Tri-Diagonal Matrix Algorithm TDMA) and the Causs-Seidel method. First, a grid line, e.g. in the r direction, is chosen. Then the dependent variables along the neighboring lines are assumed to be known from their 'latest' values. The dependent variables can now be solved along the chosen line by TDMA. This procedure is followed for all the lines in one direction and then repeated for the lines in the other directions. This method is illustrated in Fig. 3.41-1.

In general, the line-by-line iterative method has the advantage of fast convergence.

(1) The boundary condition informations from the end of the line are transmitted to the interior of the domain simultaneously.

(2) The informations from all boundaries can be quickly brought to the interior by alternating the directions in the TDMA traverse.

b. The SIMPLE Algorithm

The overall procedure, which links the momentum and continuity equations, known as SIMPLE[1] is used. It was developed by Patankar and Spalding [35] along the lines of the earlier methods by Chorin [8], Harlow and Welch [15], and Amsden and Harlow [3] etc. The procedure involves the following basic steps:

1) Solve the momentum equations using the guessed velocity and pressure fields to obtain U and V fields.
2) Solve the P' (pressure correction) equation.
3) Correct U, V, and P using the velocity-correction and pressure formulas [35].
4) Solve the equations for other scalar variables (such as T, k, and ε) if necessary.
5) Check for convergence. If not satisfied, return to step 1, and repeat the whole procedure until the solution is obtained.

3.42 ENERGY EQUATION

The discretized domain with the prescribed (temporarily known or fixed) location of interface lines, namely liquidus and solidus, is shown in Fig. 3.21-1. In general the

----

[1] SIMPLE stands for Semi-Implicit Method for Pressure Linked Equations.

discretized equations for the grid points along a chosen line can be solved either in the axial or in the radial direction. For illustration, the solving procedure is applied for all the grid lines in the radial direction.

a. Solution Domain

There are two different types of solution sub-domains in the present problem (Fig. 3.42-2). They are categorized as follows:

1) Three Distinct Phase Regions. The section consists of liquid, mushy, and solid region.
2) Two Distinct Phase Regions. The section consists of mushy and solid region only.

b. Basic Procedure

Each section is handled by solving the involved regions sequentially, from the centre line to the outer shell. The basic procedure for solving each phase region can be generalized as follows:

1) Identify the prescribed location of interface lines.
2) Fix heat flux at one boundary, and fix temperature at the other boundary. (The boundary conditions imposed for each region are listed in the next subsection.) If the

heat flux is unknown, it is computed by global energy balance of that section.

3) Solve the discretized energy equation for the region by the Tri-Diagonal Matrix Algorithm (TDMA) [19].

4) For the liquid region, no iteration is required as the heat flux at the symmetrical axis is known.

For the mushy and the solid regions, iterate the heat flux until the additional conditions along the liquidus and solidus line have been satisfied. (These conditions are listed in the following subsections.)

c. Boundary Conditions

The relevant boundary conditions for each phase region in each different section are shown in Fig. 3.42-3. The detailed description for each section is listed as follows: (For notation simplicity, the symbol "Q" is used to denote the term $\partial T/\partial r$.)

1) Three Distinct Phase Region.

			Additional Conditions
Liquid:	at $r = r_L$, (at Liquidus line)	$T = T_L$	not required
	at $r = 0$, (at centre line)	$Q = 0$	not required
Mushy:	at $r = r_S$, (at Solidus line)	$T = T_S$	not required

	at $r = r_L$,	$Q = Q_{so}$	, $T = T_S$
Solid:	at $r = r_S$,	$T = T_S$	not required
	at $r = r_{mold}$,	$Q = Q_{cool}$	T decreases radially

2) Two Distinct Phase Region.

Additional Conditions

Mushy:	at $r = r_S$,	$T = T_S$	not required
	at $r = 0$,	$Q = 0$	not required
Solid:	at $r = r_S$,	$T = T_S$	not required
	at $r = r_{mold}$,	$Q = Q_{cool}$	T decreases radially

Note that the additional condition of radially decreasing temperature is imposed to speed up the convergence for the determination of "Q".

3.43 INTERFACE LINE TRACING PROCEDURE

The problem is to trace the unknown location of solidus and liquidus lines for an imposed cooling heat flux (Qcool). Following similar treatment in energy equation, the tracing procedure can be applied either in the axial or in the radial direction; but for illustration, a cross-section in the radial direction is selected.

The procedure for tracing the solidus line in the two-distinct phase section of the domain has been selected to demonstrate the idea of the general interface line tracing procedure. Fig. 3.43-1 (a to c) show the simplified diagrams of the interface line tracing procedure. (Note that diagrams are not to scale and therefore distorted.) The symbol r_n denotes the computed radial location of the solidus line measured from the central axis for the n^{th} iteration of the computation, and the symbol r_s denotes the final converged radial location of the solidus line. The basic tracing procedure is as follows:

1) Guess the initial location of the solidus line.
2) Solve the energy equation as outlined in the previous subsection.
3) Compare the computed and imposed Qcool.
4) If necessary, adjust the location of the solidus line.
5) Repeat the steps 2 through 4 until the convergence criterion has been satisfied:

$$\left| (Qcool^i - Qcool)/Qcool^i \right| \leq \epsilon$$

where $Qcool^i$ is the imposed cooling heat flux, and Qcool is the computed one; ϵ is equal to 10^{-3} in the present computation.

3.44 OVERALL PROCEDURE

The overall procedure for the present study can be summarized as follows:

(1) Prescribe location of solidus and liquidus lines (which can be temporarily unknown or fixed).

(2) Solve the equations of motion.

(3) Solve the energy equation (with or without the interface line tracing procedure).

(4) Compute solid fraction and thermophysical properties for all regions.

(5) Solve the equations for other scalar variables (such as k and ϵ), if required.

(6) Check for convergence as stated in the following subsection 3.51; if not satisfied, return to step 1, and repeat the whole procedure until the solution is obtained.

3.5 NUMERICAL STABILITY

3.51 CONVERGENCE

To assess how the current solution approximates the exact one for each dependent variable, a convergence test is needed at the end of each iteration. The 'residual source' method is employed in the present study. From Eq.(3.24-1), the local residual source R_ϕ is defined as

$$R_\phi = \sum a_{nb}\phi_{nb} + b - a_P\phi_P$$

If the current solution exactly satisfies the equations, R_ϕ is zero; otherwise, R_ϕ is a measure of the local error. Thus, a normalized residual source $(R_\phi)_{nor}$ can be defined as

$$(R_\phi)_{nor} \sum_{\text{all nodes}} \frac{|R_\phi|}{R_{\phi,ref}} \qquad [3.51\text{-}1]$$

where $(R_\phi)_{nor}$ is typically of the order 10^{-3}, and $R_{\phi,ref}$ is an appropriately chosen reference flow quantity.

3.52 FALSE MASS SOURCE

Successive iterative procedures of the discretized equations are often prone to numerical instabilities, which result in both the non-satisfaction of mass conservation on a local and overall basis, and the oscillation rather than the convergence to constant values of the calculated values of the flow variables.

The suggested remedy [13] is to introduce a false mass source S_f as follows:

$$S_f = |\dot{m}_{net}|(\phi_P^o - \phi_P) \qquad [3.52\text{-}1]$$

where $\dot{m}_{net} = (C_e - C_w + C_n - C_s) \qquad [3.52\text{-}2]$

$\phi_P^o = \phi_P$ of previous iteration

Therefore, the final form of the discretizion equation is

$$(a_P)_f \phi_P = \sum a_{nb} \phi_{nb} + (b)_f \qquad [3.52\text{-}3]$$

where $(a_P)_f = a_P + |\dot{m}_{net}|$

$$(b)_f = b + |\dot{m}_{net}| \phi_P^o \qquad [3.52\text{-}4]$$

The introduction of this false mass source avoids singularity[9] , but has no effect on the final solution.

3.53 UNDER-RELAXATION

Under-relaxation has the effect of slowing down the changes of the solution from iteration to iteration. This effect may avoid the divergence during the course of finding the solution, especially of strong nonlinear equations. A relaxation factor F is defined by

$$\phi_P = F\,\phi_P^* + (1-F)\,\phi_P^o \qquad [3.52\text{-}5]$$

where ϕ_P denotes the final value, ϕ_P^* the value from the current iteration, and ϕ_P^o the value from the previous iteration.

The value of F must lie between 0 and 1 although the optimal value of F is usually specified empirically.

---

[9] Singularity occurs in the discretized equation when all the a_{nb} become zero.

3.5 CLOSURE

This chapter has developed a solution procedure for the present simulation. The chapter has the following main features:

(i) The partial differential equations governing the fluid flow from the previous chapter are reduced to algebraic forms by finite difference formulations through a 'finite volume' approach with a hybrid difference scheme for the fluxes.

(ii) The local thermophysical properties at the control volume boundary and those for the whole control volume are determined by using appropriate area and volume weighting factor.

(iii) The discretized equations are solved by a guess-and-correct procedure and a line-by-line iterative method. The SIMPLE algorithm is used to solve the equations of motion. Novel algorithms have been developed for solving the energy equation and tracing the unknown location of solidus and liquidus lines. Matters concerning the numerical stability are discussed.

CHAPTER 4

RESULTS AND DISCUSSIONS

4.1 INTRODUCTION

4.11 PURPOSE OF THE CHAPTER

In this chapter, a number of test cases of the continuous casting problems are presented. These test cases are solved by use of the procedure developed in Chapter 2 and 3. These examples are intended to demonstrate how the procedure, which has been outlined in general terms, can be applied to particular problems.

A uniform format for the presentation of the various test cases has been adopted. Under the heading of "Description of the Problem": the physical situation considered, the motivation for the study, and the information to be obtained, are described. In the "Detail of the Computations", the mathematical problem is outlined in terms of differential equations and boundary conditions; and the problem posed for numerical solution is also indicated. Finally, discussion of the obtained solutions is presented in "Results".

To keep the presentations as brief as possible, and to avoid needless repetition, it is useful to give several explanatory notes which apply to all the descriptions:

(1) Where possible, the notation of the previous chapters are used; only new symbols are defined.

(2) When a different physical situation is being studied, mention is made of it; otherwise, the physical situation is taken as those shown in Fig. 1.22-1.

(3) For all the test cases, a cylindrical coordinate system is used. The domain of solution and the boundary conditions are the same as those shown in Fig. 4.22-2.

(4) A 17 X 14 grid arrangement, as shown in Fig.4.22-3, is used in all the test cases.

(5) For the convergence criterion, all the computations are stopped when $(R_{\phi})_{nor}$ (Eq. 3.61-1) is less than 10^{-3}.

(6) Unless specified, the numerical values of the parameters used in the computation are those listed in Table 4.11-1.

4.12 OUTLINE OF CONTENTS

The problems have been divided into three groups, which are described by the corresponding section headings, as listed below:

(1) Scalar Analysis.

(2) Momentum Analysis.

(3) Comparison with Experiments and Previous Works.

4.2 SCALAR ANALYSIS

4.21 INTRODUCTORY REMARKS

Only the energy equation is considered in the following subsections. With the assumption of a linear profile along the radial direction, the velocity field is solved by the continuity equation. The energy equation is then solved with or without the interface line tracing procedure. The particular problems considered in this section are listed below, in the order of complexity:

(1) Testing the Solution Algorithm for Energy Equation.

(2) Effects of Variable Thermophysical Properties.

(3) Interface Line Tracing Procedure.

4.22 TESTING THE SOLUTION ALGORITHM FOR ENERGY EQ.

a. Description of the Problem

Fig. 1.22-1 shows the situation considered here. Liquid steel at a uniform temperature T_{in} and uniform velocity U_{in} enters the mold.

The velocity profile in the liquid and mushy region, location of solidus and liquidus lines, and values of solid fraction and other dependent fluid properties are all prescribed. The problem is to predict the temperature field under these prescribed conditions.

Motivation: The present solution algorithm for the energy equation has been newly developed to handle domain with multi-distinct phase regions and with unknown cooling heat flux; therefore, the main interest here is to test the algorithm.

Boundary Conditions: The domain of solution and the boundary conditions are shown in Fig. 4.22-2. In this figure, the variables x is the distances in the axial direction and r in the radial direction.

b. Results

Predictions of the temperature profiles for the whole solution domain are presented in Fig. 4.22-4. Two important observations can be made:

1) Temperature decreases in both axial and radial directions.
2) Temperature within the mushy region is bounded by the solidus and liquidus temperatures. (The values of the solidus and liquidus temperature are listed in Table 4.11-1)

4.23 EFFECTS OF VARIABLE THERMOPHYSICAL PROPERTIES

a. Description of the Problem

The situation considered here is similar to that in the previous subsection; the only difference is that the solid fraction and other thermophysical properties are now treated as parts of the solution unknown instead of being prescribed as constants. The problem here is to predict the temperature field and the solid fraction profile with the prescribed velocity profile and the prescribed location of the solidus and liquidus lines.

Motivation: The present problem is to study the effects of variable thermophysical properties on the temperature field. The present computational task is more complex than the previous one, but it provides a much more accurate representation of the actual process, since in reality the thermophysical properties and the solid fraction are functions of temperature.

b. Results

The predictions of the computed temperature profiles and the solid fraction distributions are shown in Fig. 4.23-1 and Fig. 4.23-2. Similar trends have been observed in the previous subsection; i.e., temperature fields decrease in both axial and radial directions, and are bounded by T_S and T_L within the mushy region. However, there is a higher temperature gradient near the solidus line. This finding is more readily visualized on inspection of Fig. 4.23-2, which shows that the contour line of solid fraction f_s = 0.5 is close to the solidus line instead of the previous arbitrary prescription that it lies mid-way between the solidus and liquidus lines. Further comparison of computed solid fractions with the experimental ones will be shown later in section 4.5.

4.24 INTERFACE LINE TRACING PROCEDURE

a. Description of the Problem

Fig. 1.22-1 shows the situation considered here. The problem is to trace the unknown location of solidus and liquidus lines for an imposed cooling heat flux condition. The procedure for tracing the solidus line in the two-distinct phase section of the domain has been selected to demonstrate the idea of the general interface line tracing procedure (see subsection 3.53 for detail).

b. Results

Fig. 4.24-1(a to c) shows the simplified diagrams of the solidus line tracing procedure for a section of domain at x = 15.0 cm. Various guessed locations of the solidus line during successive iterations in the computational process are shown in Fig. 4.24-1a. For instance, during the first iteration the guessed location is r_1 and the corresponding computed Q_{cool} is larger than the imposed Q_{cool}, as shown in Fig. 4.24-1b. As the number of iterations increase, the computed Q_{cool} gradually converges to the imposed Q_{cool}, as shown in Fig. 4.24-1c, and thus the designed location of solidus line is finally traced.

4.3 MOMENTUM ANALYSIS

4.31 INTRODUCTORY REMARKS

Only the equations of motion are considered in the following subsection. All thermophysical properties are prescribed here. Furthermore, the location of the solidus and liquidus lines are also specified. Two particular problems are considered in the present section, and they are listed as follows:

(1) Testing the Solution Algorithm for Equations of Motion.
(2) Application to Nozzle Configuration

4.32 TESTING THE SOLUTION ALGORITHM FOR EQS. OF MOTION

a. Description of the Problem

Fig. 1.22-1 shows the situation considered here. The problem is to predict the velocity profile in the liquid and mushy region with a uniform inlet velocity condition. No thermal buoyancy effects are considered. (These effects are considered in the next subsection, 4.33.) Both laminar and turbulent cases are considered for the conditions mentioned.

Motivation: The present solution algorithm for the equations of motion is newly developed to handle the multi-phase domain; therefore, the main interest here is to test the validity of the algorithm.

b. Results

Fig. 4.32-1a shows the velocity profile at various sections of the solution domain. The velocity field is perhaps more readily visualized, if the velocities are considered relative to the casting speed (Fig. 4.32-1b). Two comments can be made:

1) The absolute velocity profile seems to be uniform at various sections of the domain.
2) If relative velocities are considered; however, one can observe that the velocities in the liquid region are larger than those in the solid region.

Since the density of solid steel is greater than that of liquid steel, the velocity of liquid steel must be greater than that of solid metal in order to satisfy the mass conservation. Similar trends are also observed for the turbulent case (Fig. 4.32-1c and d).

4.33 APPLICATION TO NOZZLE CONFIGURATION

a. Description of the Problem

Liquid steel at a uniform temperature and velocity enters the mold through a straight axial nozzle, as shown in Fig. 4.33-1. The problem is to predict the velocity profile in the liquid and mushy region with this nozzle configuration. Buoyancy effects are included in the study. Both laminar and turbulent cases are being considered.

Motivation: The purpose of the present problem is to test the applicability of the newly developed model and to obtain some performance information of industrial interest.

Boundary Conditions: The domain of solution, the grid arrangement, and the boundary conditions are shown in Fig. 4.33-2. The straight axial nozzle considered here is an axisymmetric one with a 3-cm diameter.

b. Results

Fig. 4.33-3a shows the normalized[10] streamline pattern while Fig. 4.33-3b shows its corresponding velocity fields. The solidus line on these figures is indicated by the curved solid line. From the inspection of these figures, one notices a back-flow region in the vicinity of the solidification front. The trend of the result agrees with the findings in previous publications [23,57], that this region of reverse flow is inherently associated with the use of a straight nozzle.

4.4 COMPARISON WITH EXPERIMENT AND PREVIOUS WORK

The present section deals with the examination of the appropriateness and validity of the developed model. The numerical values for the parameters used in computation are listed in Table 4.11-1. They are selected to allow a direct comparison with the plant-scale measurements and with the previous computational works.

The physical situation considered here is shown in Fig. 1.22-1, and the boundary condition is shown in Fig. 4.22-2.

---

10 In the present problem the normalized stream function ψ'' is defined as: ψ / ψ_{max}

Fig. 4.42-1 shows the comparison of the computed profiles of solid fraction with the experimental measurements of the shell thickness reported by Ushijima [52]. In the figure, the experimental data are designated by the symbol '*'. The agreement between measurements and prediction is reasonably good, since these data appear to be well represented by a curve corresponding to a solid fraction of 0.5, as computed by the present model.

Fig. 4.43-1 shows the temperature profiles for the solution domain. The full line corresponds to the temperature profile computed by previous work [4]. The broken line represents the temperature profile computed by the present model. Finally, the dotted lines T_S correspond to the location of the solidus line, and T_L of the liquidus line. The curves indicate that the prediction by the present model are more realistic since the predicted temperature in the mushy region is bounded by the solidus and liquidus temperatures. In previous work some of the predicted temperatures in the mushy region were out of bounds. This can be explained by the fact that in previous work the compatibility conditions along the interface lines have not been imposed.

CHAPTER 5

CONCLUSIONS AND RECOMMENDATIONS

5.1 SUMMARY OF CONTRIBUTIONS AND FINDINGS

5.11 MATHEMATICAL CONTRIBUTIONS

A generalized model has been formulated to describe a multi-phase domain with phase change. The effects of the turbulent fluid flow with buoyancy and the mechanisms of heat and mass transfer have been considered for the different phase regions involved. The main contribution of the present formulation is that the interaction of fluid flow and heat flow can be investigated in a multi-phase region.

Varied thermophysical properties have been considered. An original latent heat treatment has been proposed, which does not involve any assumption about the heat release profile. Solid fraction treatment has been proposed to describe the two-phase effects.

5.12 NUMERICAL CONTRIBUTIONS

The governing multi-phase PDEs have been converted into algebraic forms suitable for numerical solutions by the newly developed discretization method, which is based on the finite volume method (FVM). The significance of this discretization method is its ability to discretize the differential equation for a multi-phase control volume.

Two new solution algorithms have also been developed: one is for solving the energy equation with phase change; the other for tracing the unknown location of the interface lines. The equations of motion have been solved by a modified SIMPLE algorithm.

5.13 COMPUTATIONAL RESULTS

To demonstrate the applicability of the present models, they have been applied to some test cases of continuous casting of steel. The predicted solid fraction is found to be in reasonably good agreement with measurements. The predicted temperature profiles are found to be physically realistic as the temperature within the mushy region is bounded by the liquidus and solidus temperatures.

The computed fluid flow patterns within the molten pool appear physically reasonable. For the case with the use of an axial-flow nozzle configuration, the flow patterns also provide an improved insight into the behaviour of a continuous casting system.

5.2 SUGGESTIONS FOR FURTHER WORK

The present approach, which takes into account both multi-phase fluid flow and phase change phenomena, shows considerable promise. It is worthwhile to comment briefly on the areas where further work would be needed:

(1) Further Coupled Solution

In spite of the additional numerical complexities that are expected to be involved, it would be highly desirable to couple all the governing equations, namely continuity, momentum, energy, interface, and variable thermophysical properties.

(2) Additional Configurations

The effects of different inlet conditions should also be investigated; for example, the use of a radial-flow nozzle, the speed of casting, and the size of the mold.

(3) Additional Phenomena

The boundary conditions for heat transfer at the cooling surfaces were rather simplified. Further development in these area could include the additional heat transfer mechanisms, such as the film boiling and forced convection.

(4) Further Model Verification

To verify the developed models further, test cases could be carried out on other simplified processes, such as the melting of pure metal and the freezing of water.

5.3 CONCLUDING REMARKS

Although considerable mathematical and numerical complexities are involved, the multi-phase model developed here is still a simplification of the actual process. As the development and testing of the computer code is still continuing, further experimental comparisons would be highly desirable to confirm the numerical predictions.

With some modification of the present models, they can be extended to simulate other multi-phase problems with or without phase change. Finally, the present mathematical and numerical models may be a helpful complement to other experimental efforts focussed on a better understanding of the multi-phase and phase change phenomena.

Constants in the Turbulence Model

C_1	C_2	C_μ	C_D	σ_K	σ_ε	σ_t
1.44	1.92	0.09	1.0	1.0	1.3	0.9

TABLE: 2.23-1 CONSTANTS IN THE TURBULENCE MODEL (23)

CONSERVATION OF	ϕ	Γ_ϕ	S_ϕ
MASS	1	0	0
AXIAL MOMENTUM	U	μ_{eff}	$\partial/\partial x(\mu_{eff}\partial U/\partial x) + 1/r(r\mu_{eff}\partial V/\partial x) - \partial P/\partial x$
RADIAL MOMENTUM	V	μ_{eff}	$\partial/\partial x(\mu_{eff}\partial V/\partial r) + 1/r\,\partial/\partial r(r\mu_{eff}\partial V/\partial r) - 2\mu_{eff} V/r + U^2\rho/r - \partial P/\partial r$
ENERGY	T	$\mu/\sigma + \mu_t/\sigma_t$	S_h
KINETIC ENERGY	K	μ_{eff}/σ_k	$G_k - \rho\varepsilon C_D$
DISSIPATION RATE	ε	$\mu_{eff}/\sigma_\varepsilon$	$\varepsilon/k(C_1 G_k - C_2\rho\varepsilon)$

WHERE

$$G_k = \mu_{eff}\{2[(\partial U/\partial x)^2 + (\partial V/\partial r)^2 + (V/r)^2] + (\partial U/\partial r + \partial V/\partial x)^2 + (\partial U/\partial x)^2 + (\partial U/\partial r - U/r)^2\}.$$

TABLE: 2.24-1 DEFINITION OF ϕ, Γ, S_ϕ, of EQUATION 2.24-3

THERMAL CONDUCTIVITY (FROM FIG: 2.41-1)

0° to $1640^\circ F$,	$K = 28.58 - 0.00722\ (T - 100.0)$
1640° to $2640^\circ F$,	$K = 17.3 + 0.0012\ (T - 1640.0)$
2640° to $2730^\circ F$,	$K = 18.5 - 0.0389\ (T - 2640.0)$
$>2730^\circ F$,	K is constant at 15.0

(T is in ^0F and K in BTU/hr - ft - ^0F)

To convert K to S.I. units, multiply by 1.7307.

TABLE: 2.41-1 CONSTANTS IN THE LINEAR RELATIONSHIPS FOR CONDUCTIVITY (38)

SPECIFIC HEAT (FROM FIG: 2.41-2)

0° to $800^\circ F$,	$C_p = 0.118 + 0.00005\ (T - 200.0)$
800° to $1300^\circ F$,	$C_p = 0.148 + 0.000148\ (T - 800.0)$
1300° to $1800^\circ F$,	$C_p = 0.222 - 0.000108\ (T - 1300.0)$
1800° to $2640^\circ F$,	$C_p = 0.168 + 0.0000381\ (T - 1800.0)$
2640° to $2730^\circ F$,	$C_p = 0.20 + 0.01/90\ (T - 2640.0)$
$>2730^\circ F$,	C_p is constant at 0.21

(T is in ^oF and C_p in BTU/lb-^oF)

To convert C_p to S.I. units, multiply by 4186.9

TABLE: 2.41-2 CONSTANTS IN THE FUNCTIONAL RELATIONSHIPS FOR SPECIFIC HEAT (33)

PHYSICAL DATA USED IN THE COMPUTATION

Diameter of Mold	= 11.5 cm
Diameter of Nozzle	= 3 cm
Mold length	= 50 cm
Casting Speed	= 3.17 cm/s
Casting Temperature	= 1550°C

THERMAL PROPERTIES OF LOW CARBON STEEL

Density : Liquid: 7200.0 Kg/m^3

Solid : 7480.6 Kg/m^3

Liquidus Temperature : 1498.8°C (2730.0°F)

Solidus Temperature : 1448.8°C (2640.0°F)

Latent Heat of Fusion : 272.1 KJ/Kg

Viscosity $\mu_{lam} = 5.0 \times 10^{-3}$ Kg/m-sec

TABLE: 4.11-1 PHYSICAL AND THERMAL PROPERTIES DATA USED IN THE PRESENT COMPUTATION (4)

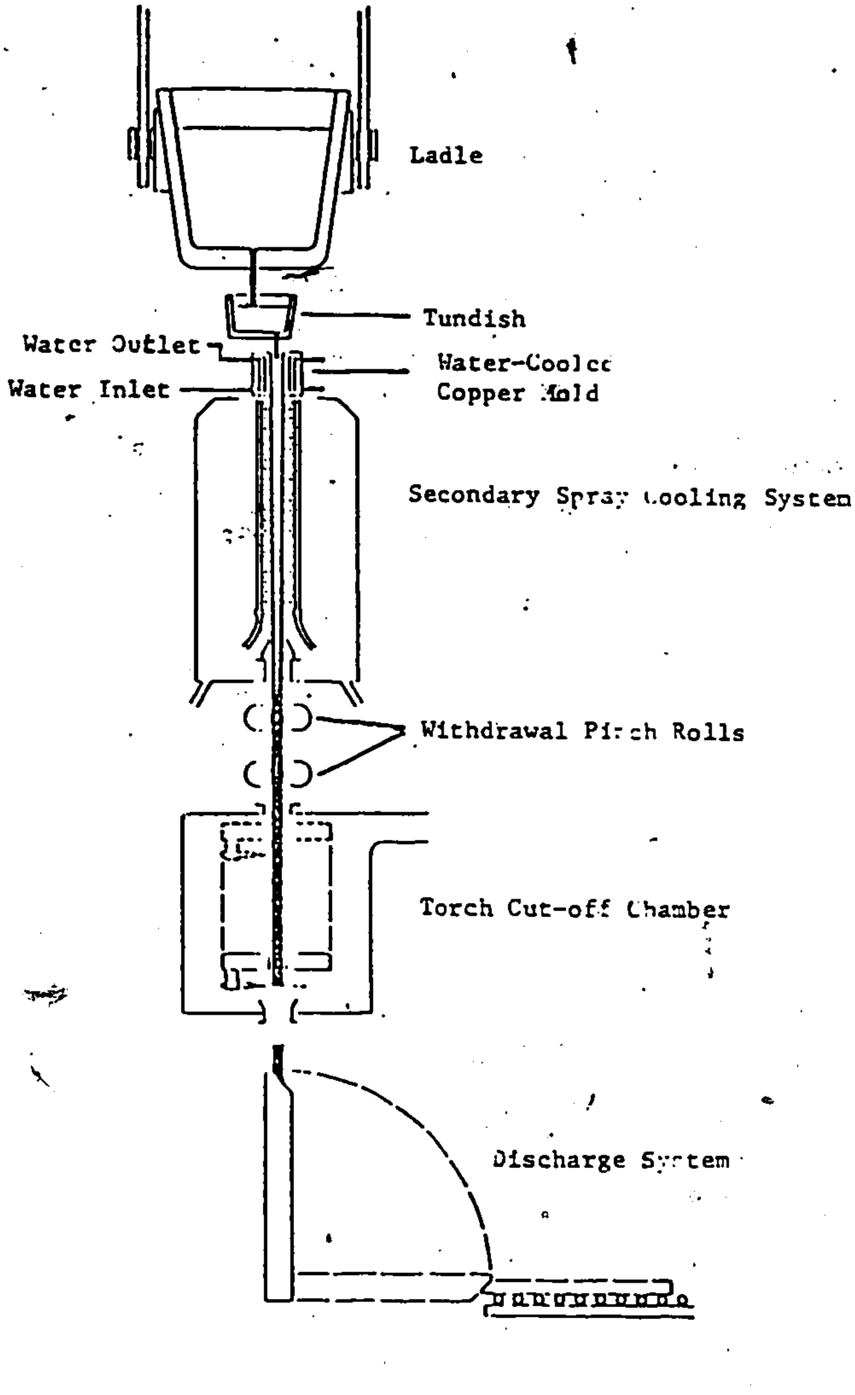

FIG: 1.21-1 ARRAGEMENT OF CONTINUOUS CASTING MACHINE AT ATLAS STEEL

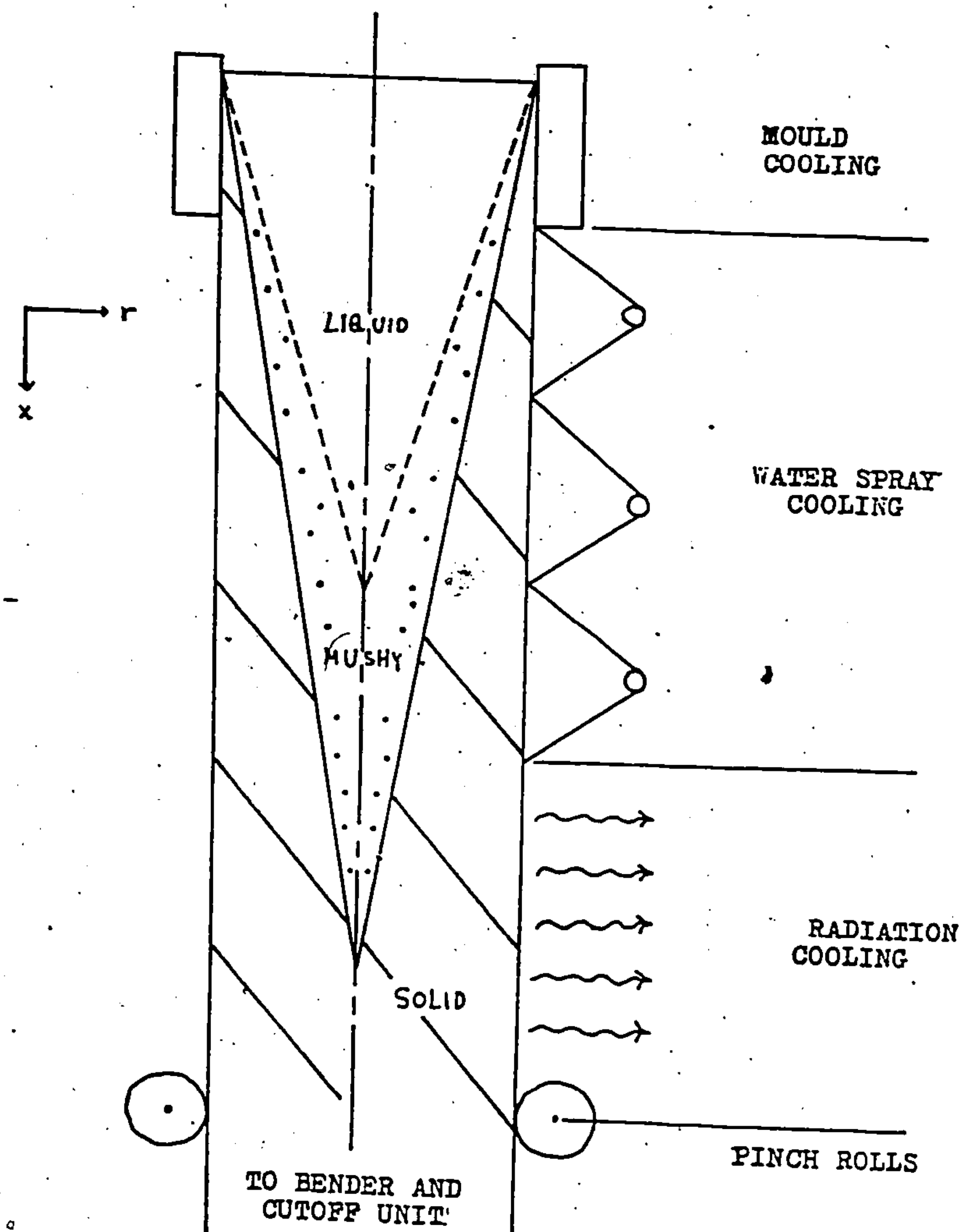

FIG: 1·22-1 SCHEMATIC DIAGRAM OF A CONTINUOUS CASTING SYSTEM

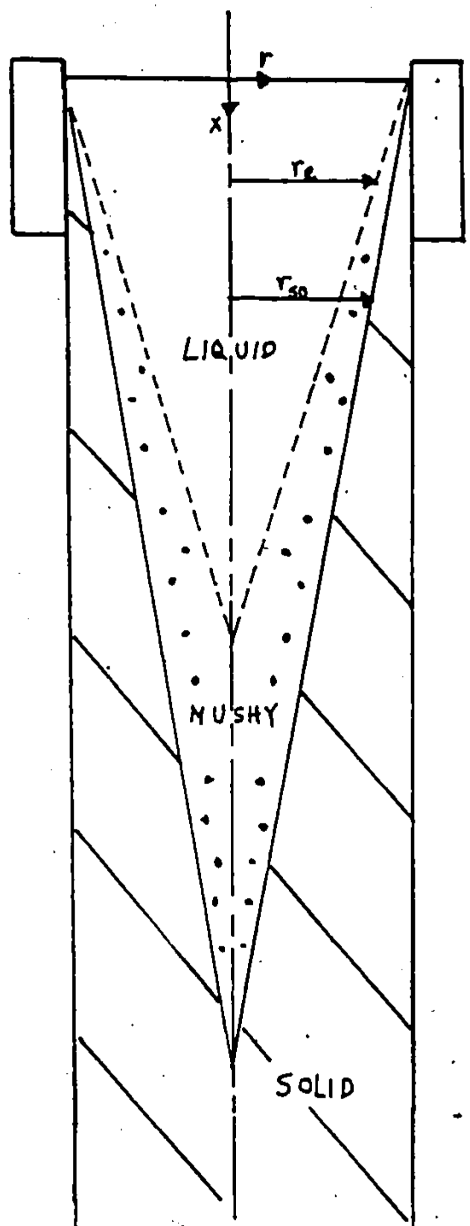

FIG: 2.31-1 RADIUS r_l OF THE LIQUIDUS INTERFACE AND RADIUS r_{so} OF THE SOLIDUS INTERFACE

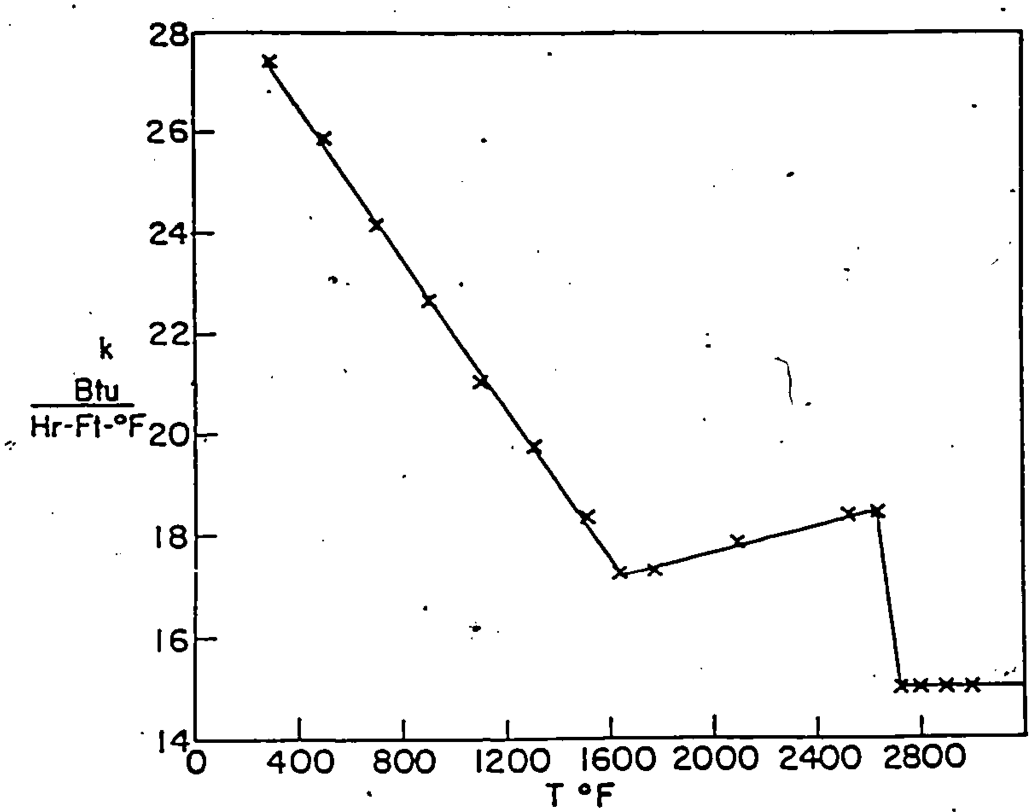

FIG: 2.41-1 CORRELATIONS FOR THE THERMAL CONDUCTIVITY OF LOW CARBON STEEL (38)

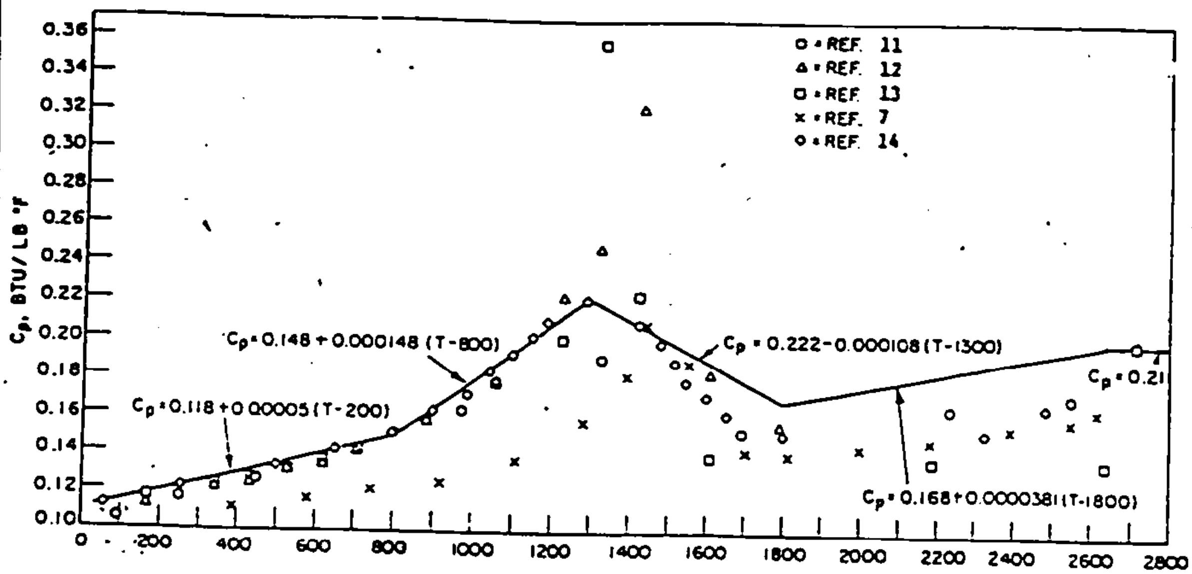

FIG: 2.41-2 SELECTED DATA AND FUNCTIONAL RELATIONSHIPS FOR SPECIFIC HEAT OF LOW CARBON STEEL (38)

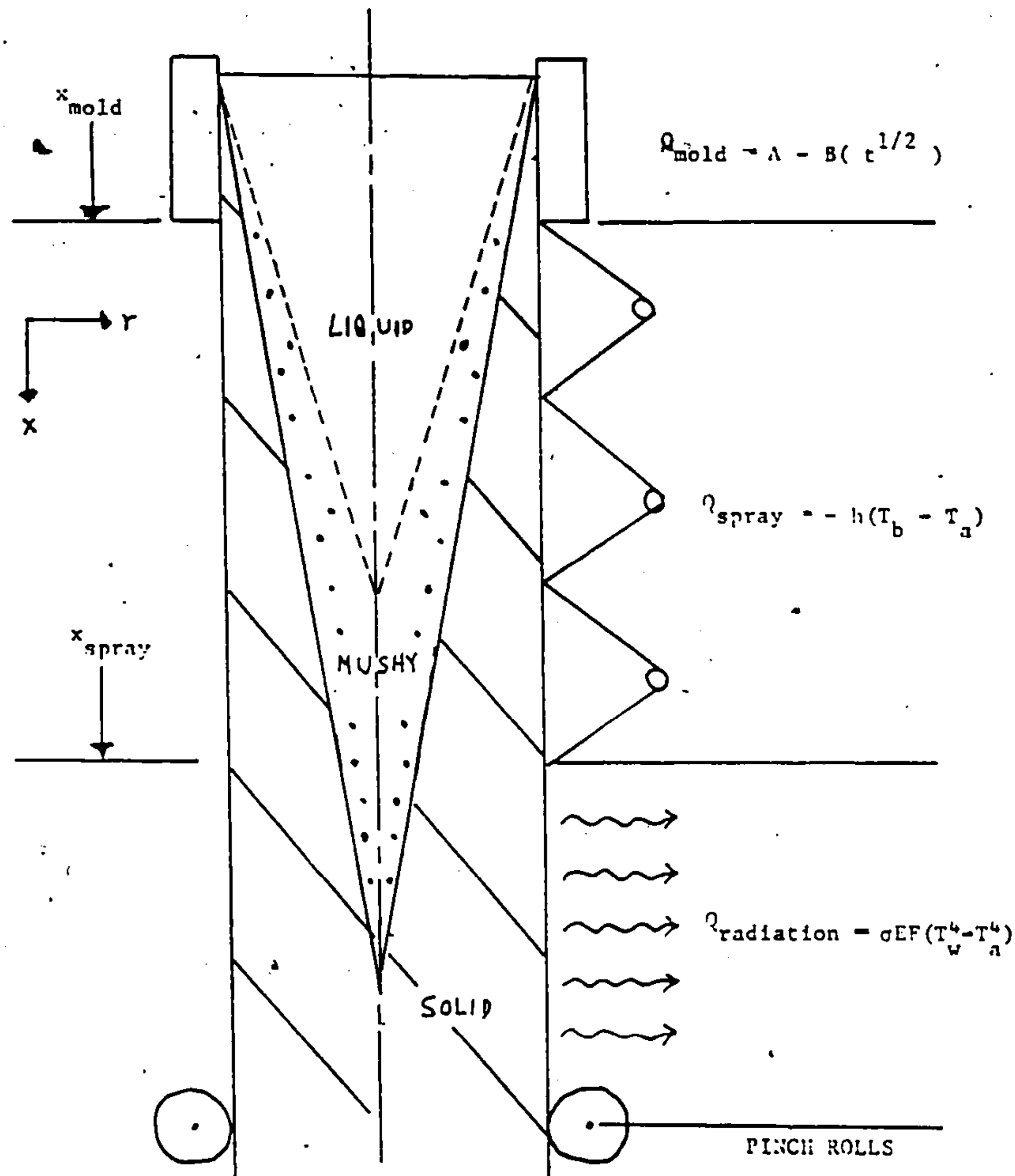

FIG: 2.42-1 DIFFERENT CONDITIONS AT VARIOUS COOLING BOUNDARIES WITH PROCESS OF CONTINUOUS CASTING

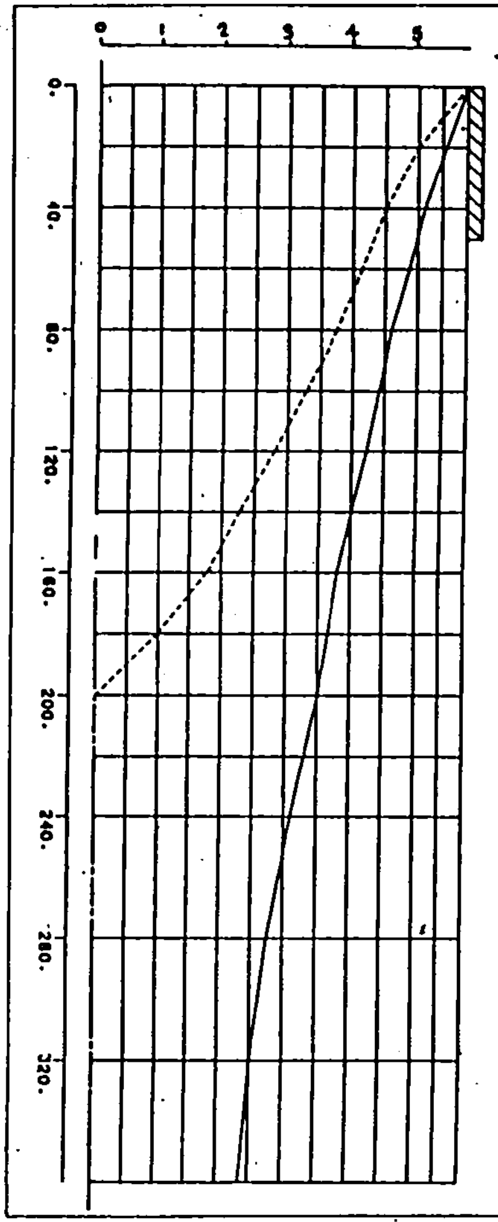

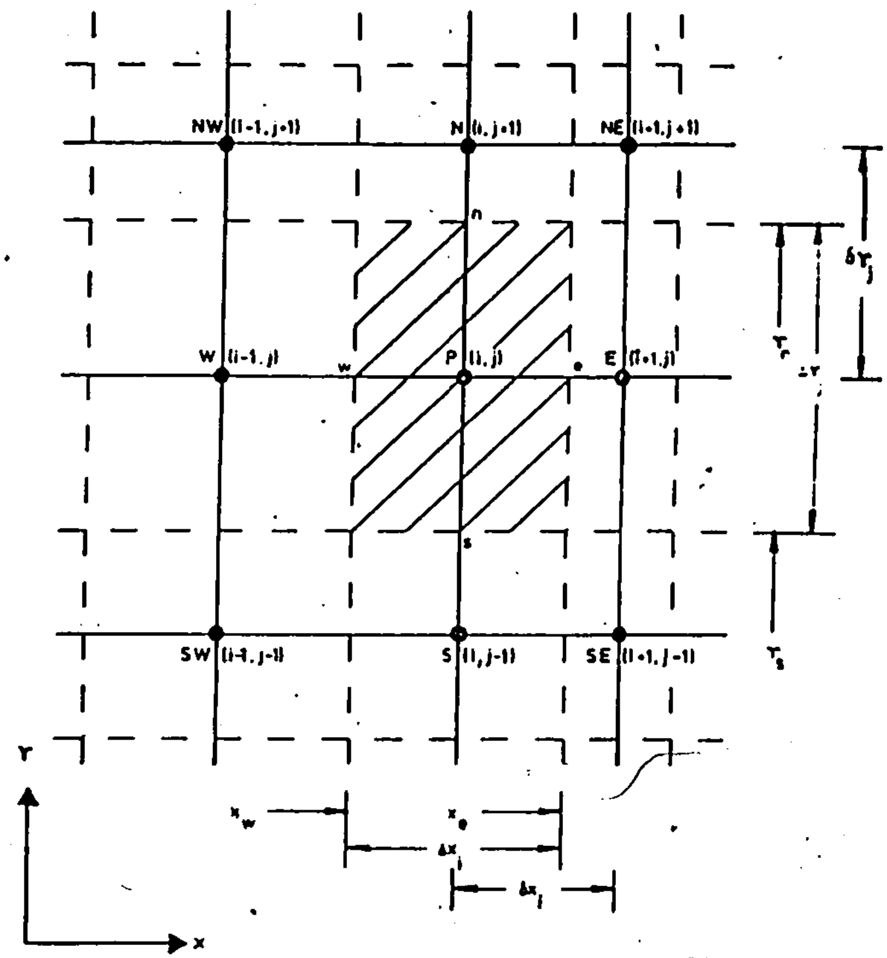

Fig: 3.21-1 GRID, FINITE VOLUMES AND NOTATIONS FOR A TYPICAL FINITE VOLUME

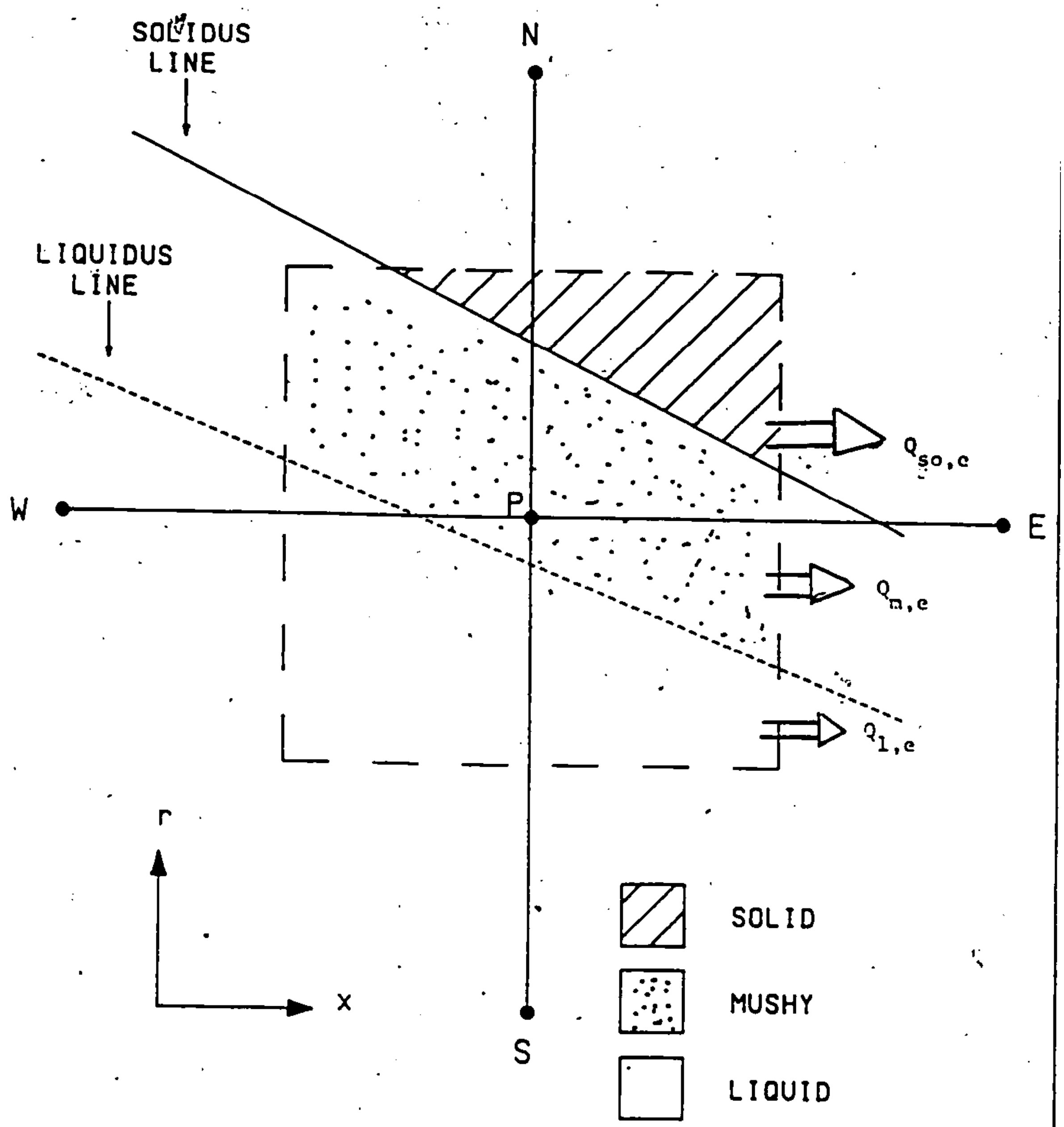

(NOTE: ALL POINTS ARE MEASURED FROM THE AXES OF THE CYLINDRICAL COORDINATES SYSTEM)

FIG: 3.21—2 TOTAL TRANSPORT ON EAST BOUNDARY OF A MULTIPHASE CONTROL VOLUME

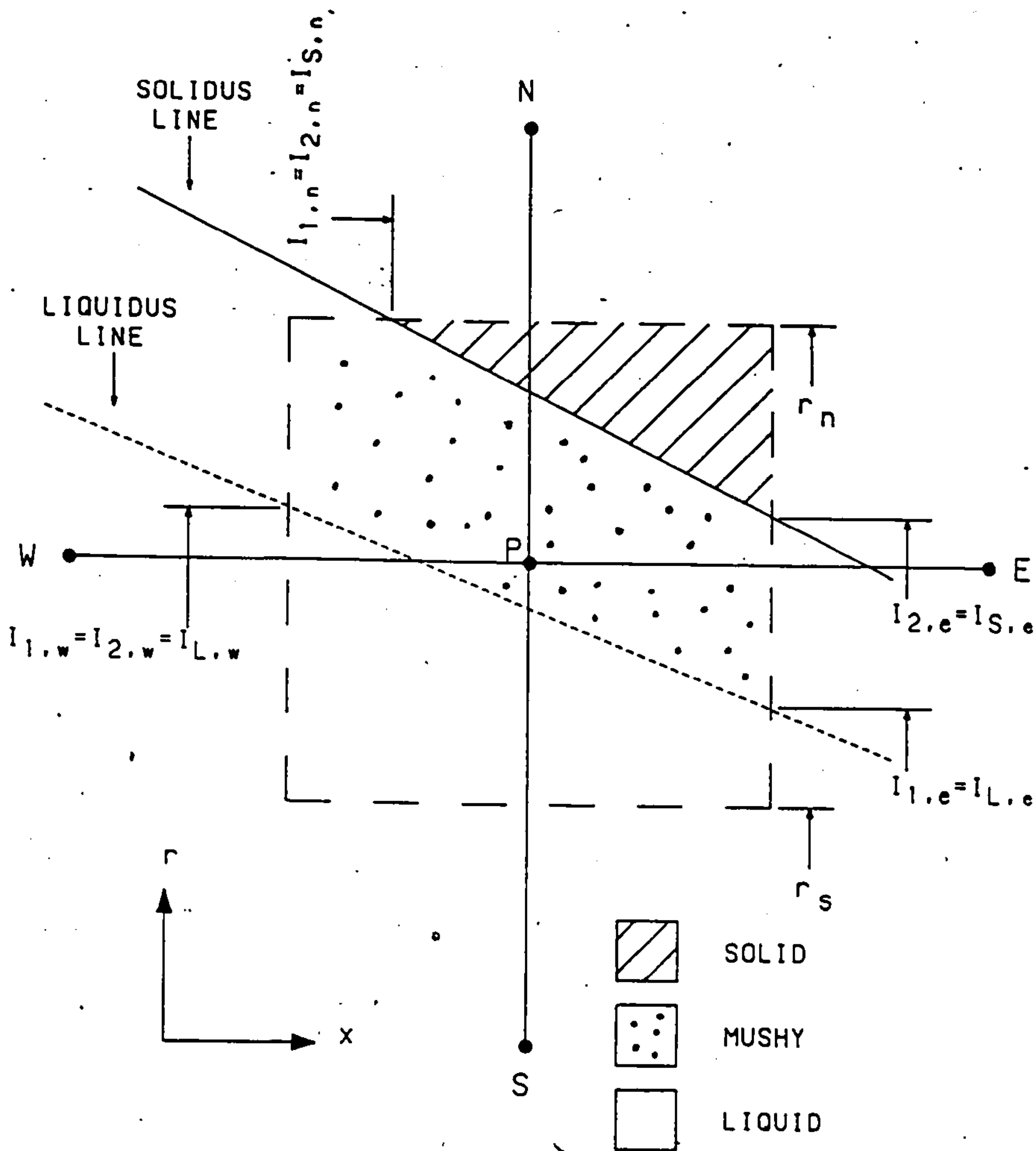

(NOTE: ALL POINTS ARE MEASURED FROM THE AXES OF THE CYLINDRICAL COORDINATES SYSTEM)

FIG. 3.22-1: A TYPICAL MULTIPHASE CONTROL VOLUME

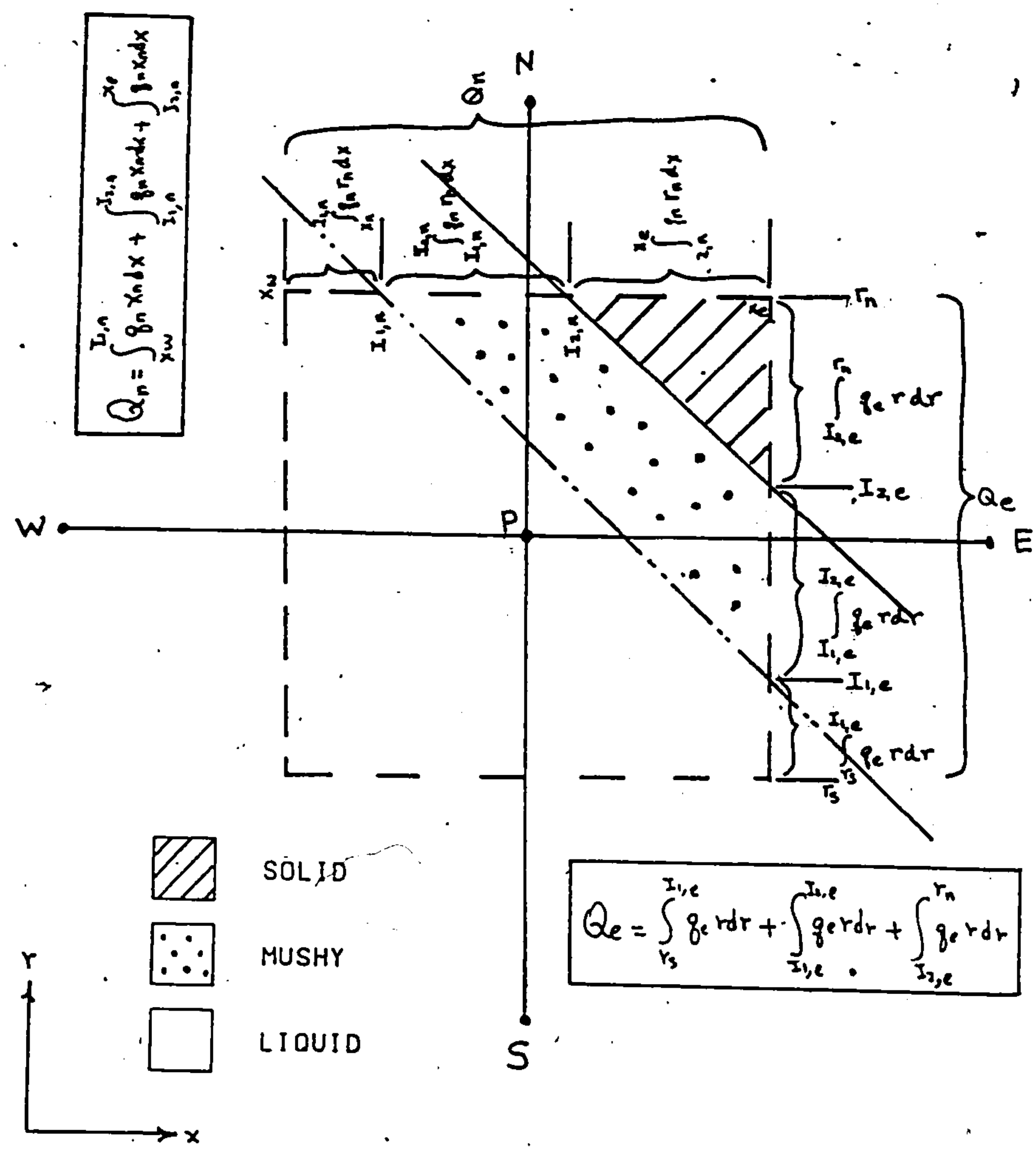

(NOTE: ALL POINTS ARE MEASURED FROM THE AXES OF THE CYLINDRICAL COORDINATES SYSTEM)

FIG: 3.23-1 TOTAL TRANSPORT ON EAST AND NORTH BOUNDARY OF A MULTIPHASE CONTROL VOLUME

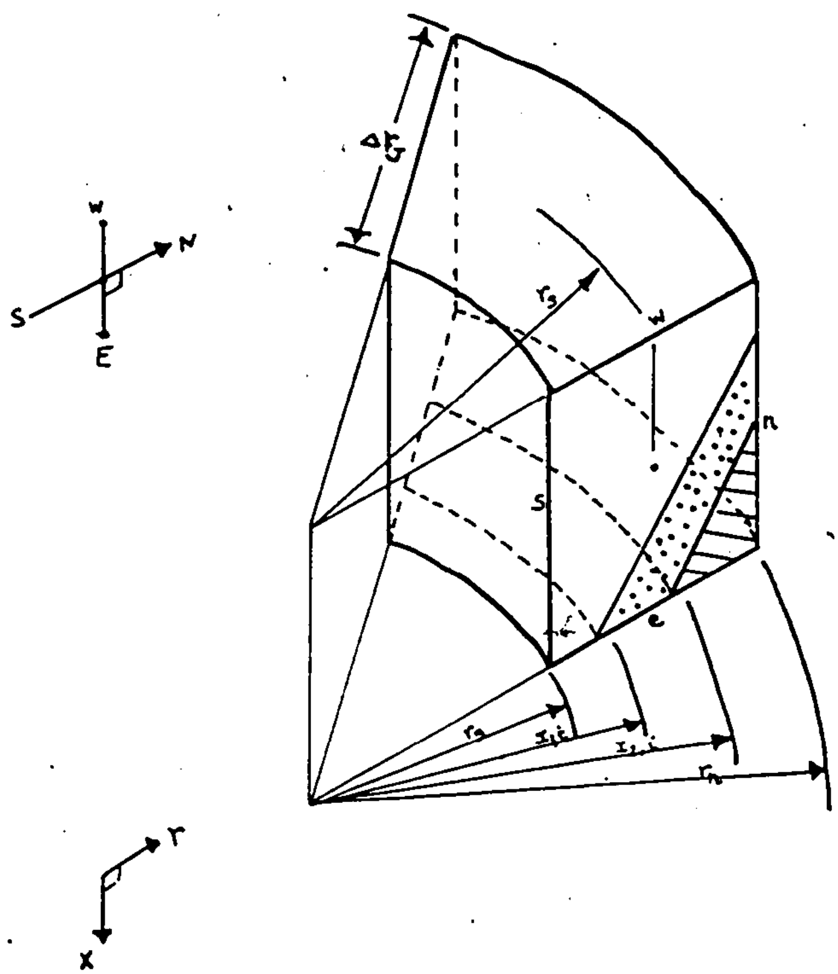

FIG: 3.23-2 AXIAL DIMENSIONLESS AREA RATIO ON THE EAST BOUNDARY OF A MULTIPHASE CONTROL VOLUME

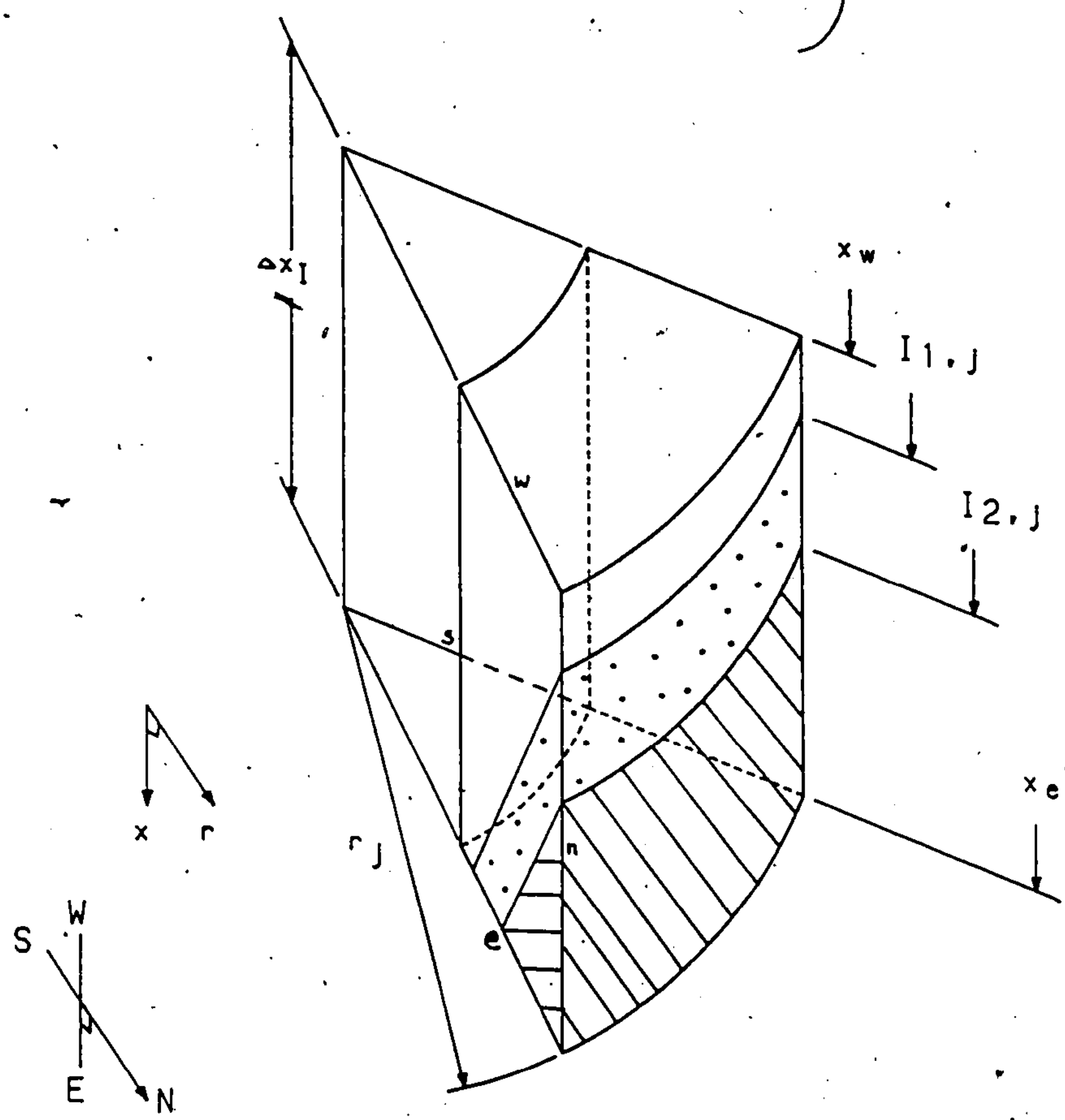

FIG: 3.23-3 RADIAL DIMENSIONLESS AREA RATIO ON THE NORTH BOUNDARY OF A MULTIPHASE CONTROL VOLUME

(1) SINGLE REGION CONTROL VOLUME

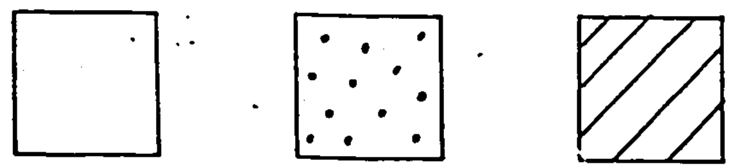

(2) LIQUID - MUSHY REGION CONTROL VOLUME

(3) SOLID - MUSHY REGION CONTROL VOLUME

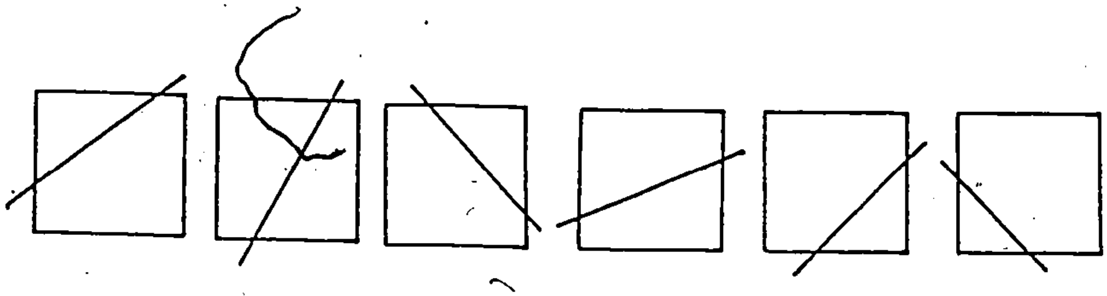

(4) LIQUID - MUSHY - SOLID CONTROL VOLUME

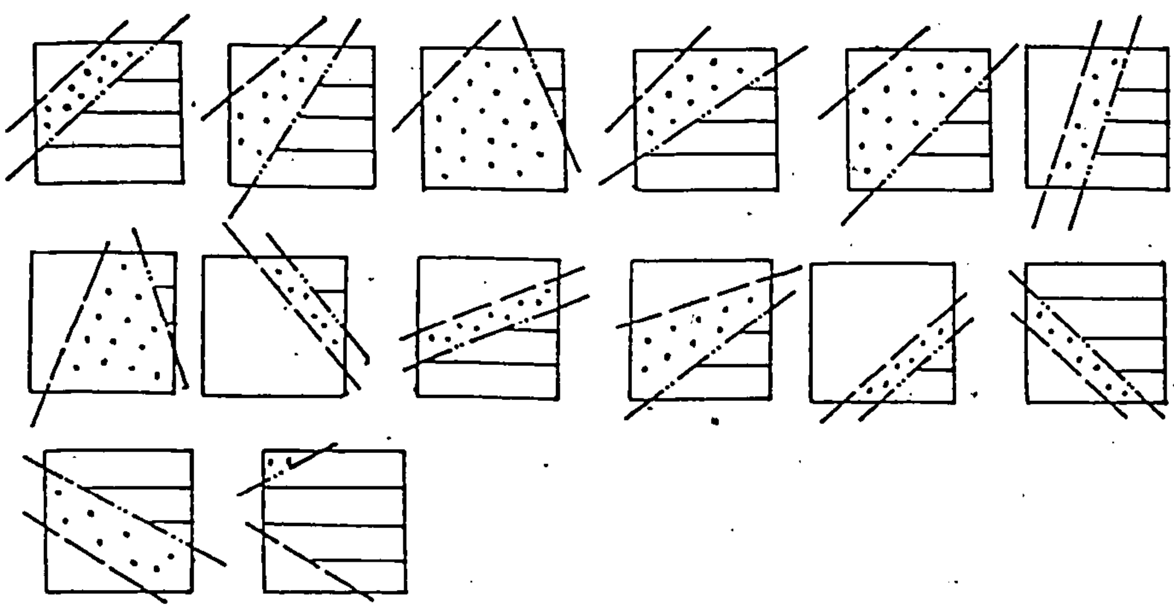

FIG: 3.23-4 FOUR POSSIBLE TYPES OF CONTROL VOLUMES DUE TO DIFFERENT PHASE REGIONS INVOLVED

P : NODAL POINT P

E : NODAL POINT AT EAST SIDE

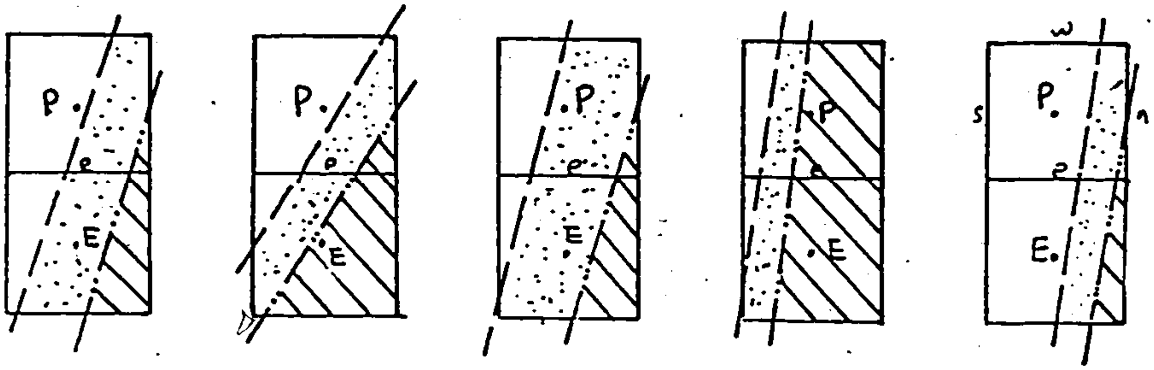

FIG: 3.32-1a LIQUIDUS AND SOLIDUS LINES INTERCEPT THE EAST BOUNDARY OF THE CONTROL VOLUME P

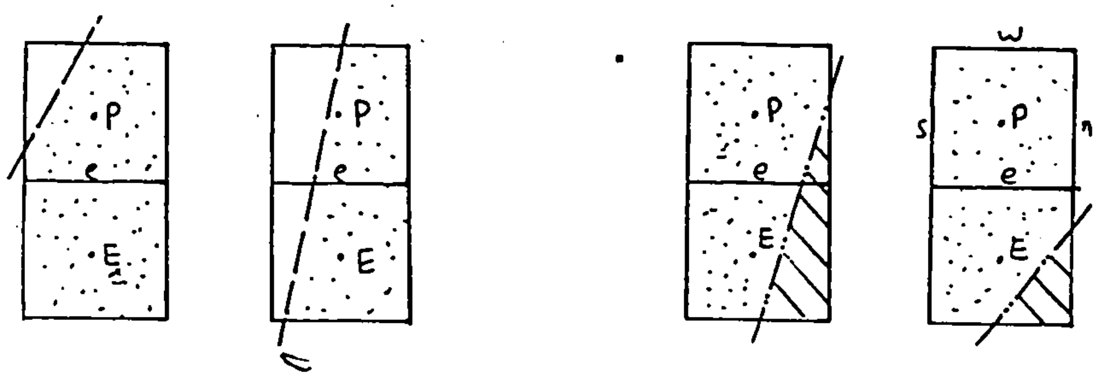

FIG: 3.32-1b CENTERED P AND EAST E NODAL TEMPERATURES LIE IN THE MUSHY REGION

NOTE: CONTROL VOLUMES ARE ROTATED SO THAT " e " IS HORIZONTAL

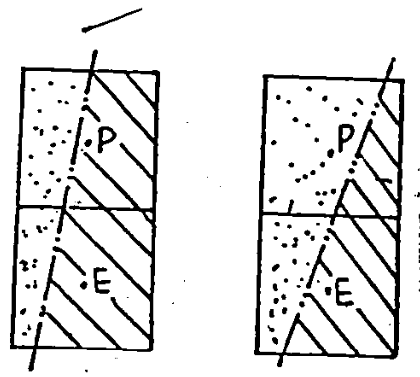

FIG: 3.32-1c CENTERED P AND EAST E NODAL TEMPERATURES LIE INSIDE THE SOLID REGION; OR P IN MUSHY AND E IN SOLID REGION

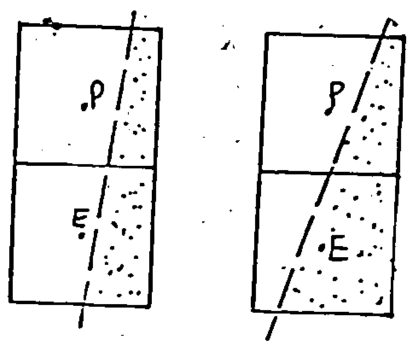

FIG: 3.32-1d CENTERED P AND EAST E NODAL TEMPERATURES LIE OUTSIDE THE LIQUID REGION; OR P IN LIQUID AND E IN MUSHY REGION

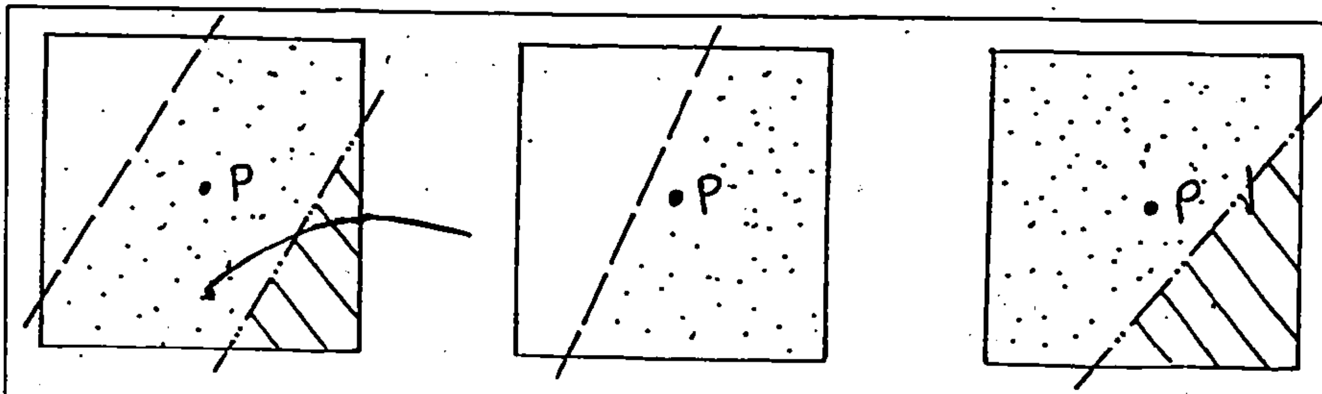

FIG: 3.33-1a, NODAL POINT P LIES IN THE MUSHY REGION

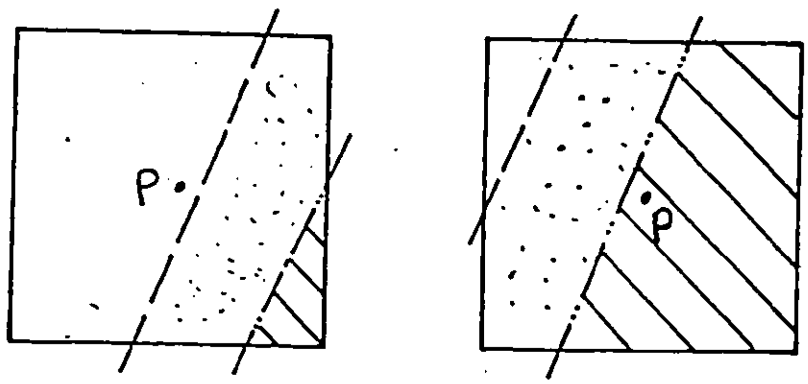

FIG: 3.33-1b BOTH LIQUIDUS AND SOLIDUS LINES INTERCEPT THE CONTROL VOLUME; AND P LIES OUTSIDE THE MUSHY REGION

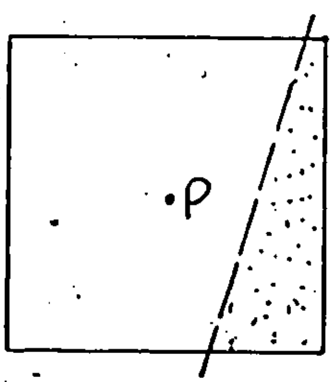

FIG: 3.33-1c ONLY LIQUIDUS LINE INTERCEPTS THE CONTROL VOLUME; AND P LIES INSIDE THE LIQUID REGION

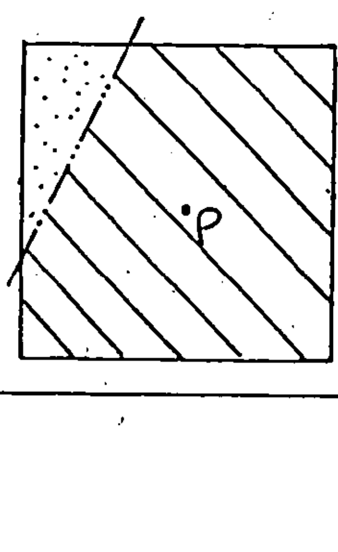

FIG: 3.33-1d ONLY SOLIDUS LINE INTERCEPTS THE CONTROL VOLUME; AND P LIES INSIDE THE SOLID REGION

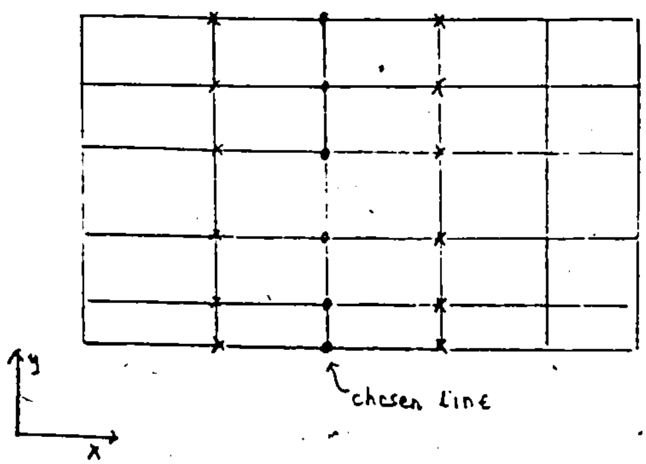

FIG: 3.41-1 REPRESENTATION OF THE LINE-BY-LINE METHOD

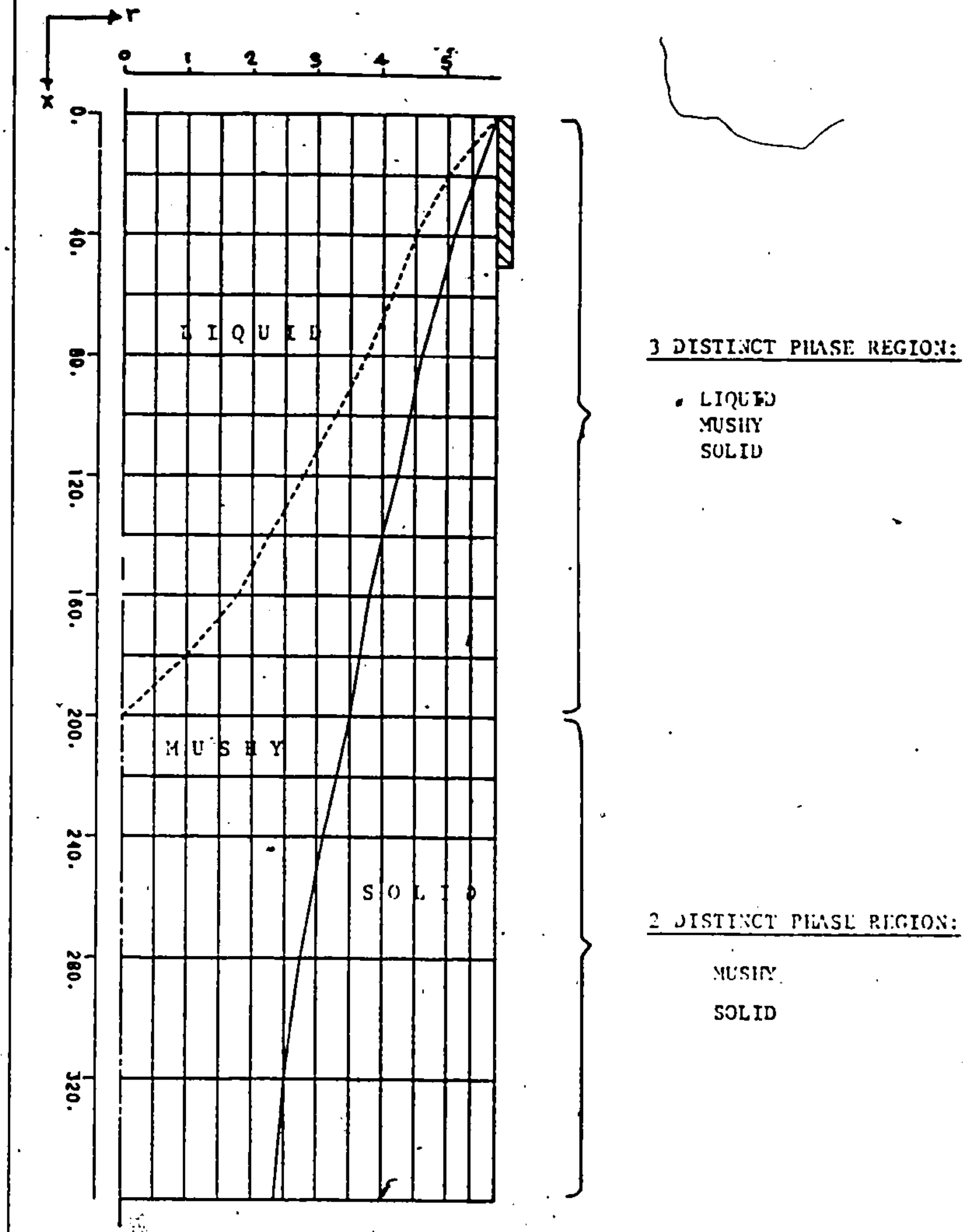

FIG: 3.42-2 2 DIFFERENT TYPES OF SOLUTION SUB-DOMAINS

BOUNDARY CONDITION

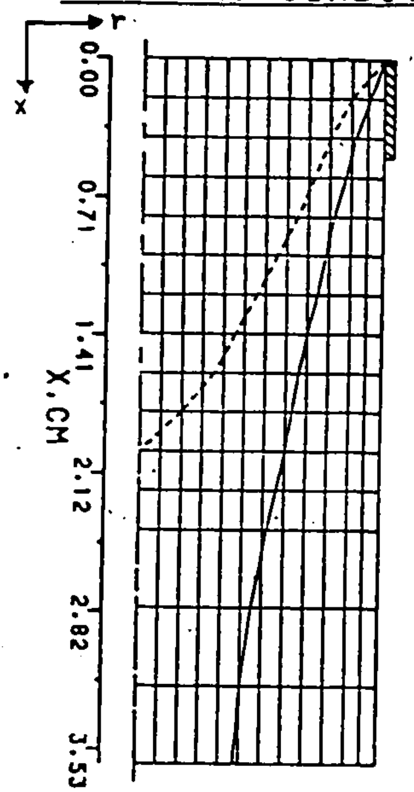

a. 3 DISTINCT PHASE REGION

LIQUID:	AT $R = R_L$,	$T = T_L$
	AT $R = 0$,	$(\partial T/\partial r) = 0$
SOLID:	AT $R = R_S$,	$T = T_S$
	AT $R = R_{MOLD}$,	$(\partial T/\partial r)=(\partial T/\partial r)_{cool}$
MUSHY:	AT $R = R_L$,	$T = T_L$
	AT $R = R_S$,	$(\partial T/\partial r)=(\partial T/\partial r)_{so}$

b. 2 DISTINCT PHASE REGION

SOLID:	AT $R = R_S$,	$T = T_S$
	AT $R = R_{MOLD}$,	$(\partial T/\partial r)=(\partial T/\partial r)_{cool}$
MUSHY:	AT $R = R_S$,	$T = T_S$
	AT $R = 0$,	$(\partial T/\partial r) = 0$

FIG: 3.42-3 BOUNDARY CONDITIONS FOR EACH PHASE REGION IN DIFFERENT SECTIONS OF THE DOMAIN

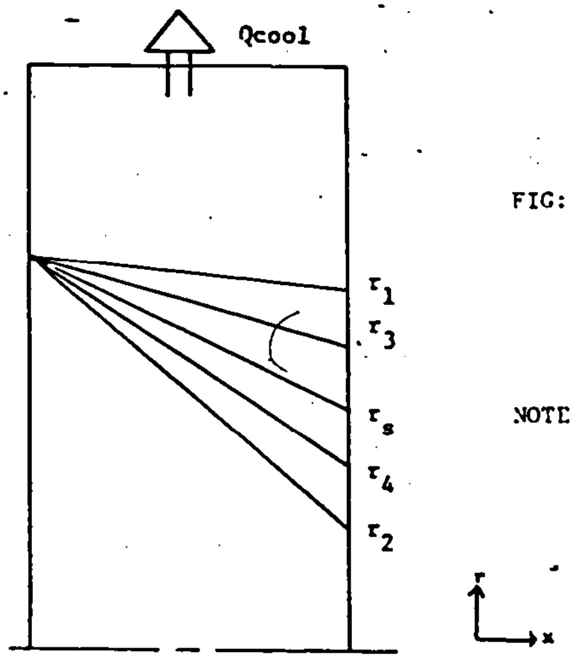

FIG: 3.43-1a A TYPICAL SECTION ALONG THE VERTICAL AXIS WITH VARIOUS GUESSED LOCATION OF SOLIDUS LINE

NOTE: ILLUSTRATION OF A CUT PERPENDICULAR TO THE CAST

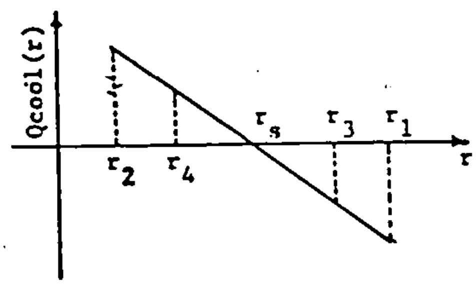

FIG: 3.43-1b PLOT OF COMPUTED Qcool VS RADIAL DISTANCE r

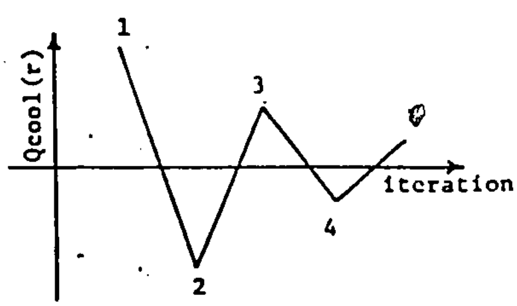

FIG: 3.43-1c PLOT OF COMPUTED Qcool VS NUMBER OF ITERATION

SIMPLIFIED DIAGRAMS TO ILLUSTRATE THE LINE TRACE PROCEDURE
(NOT TO SCALE)

FIG: 3.43-1 INTERFACE LINE TRACING PROCEDURE

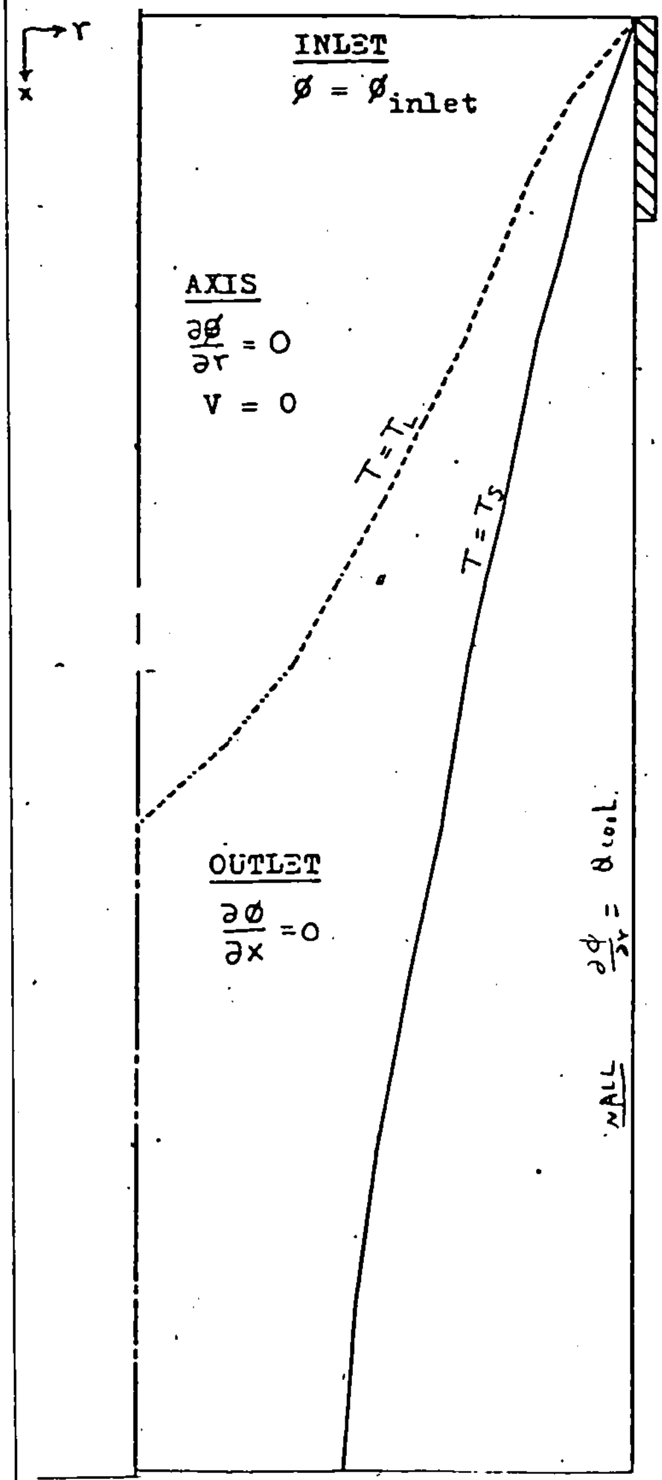

FIG: 4.?22-2 THE DOMAIN OF SOLUTION AND THE BOUNDARY CONDITIONS

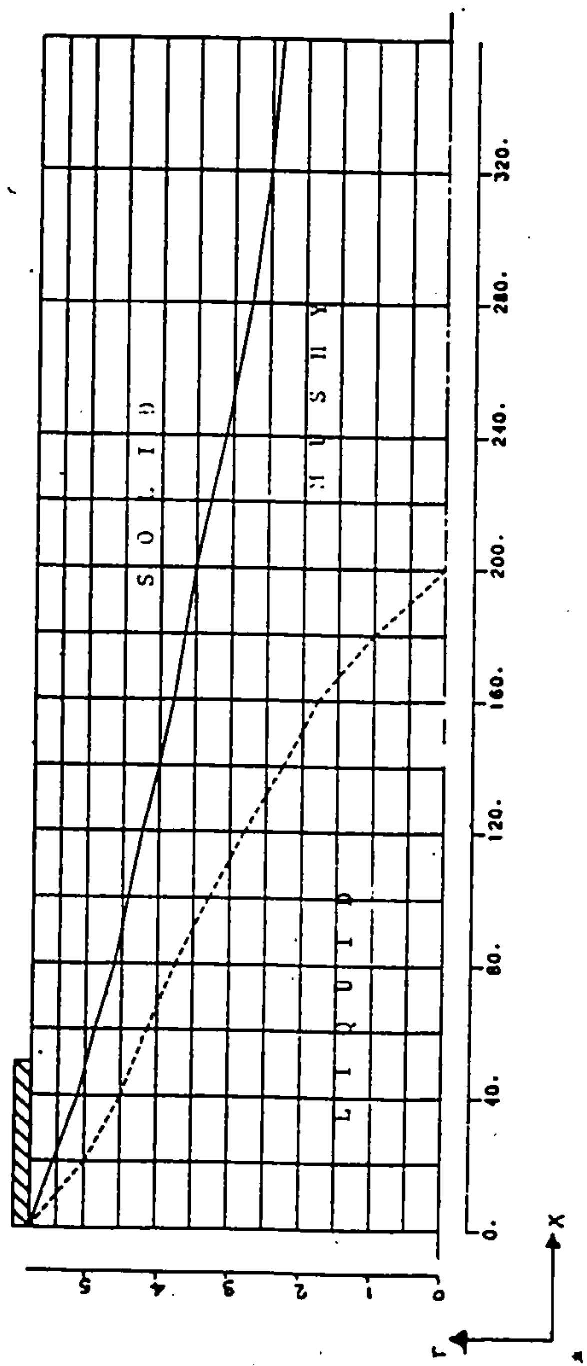

FIG: 4.22-3 A 17 X 14 GRID ARRANGEMENT

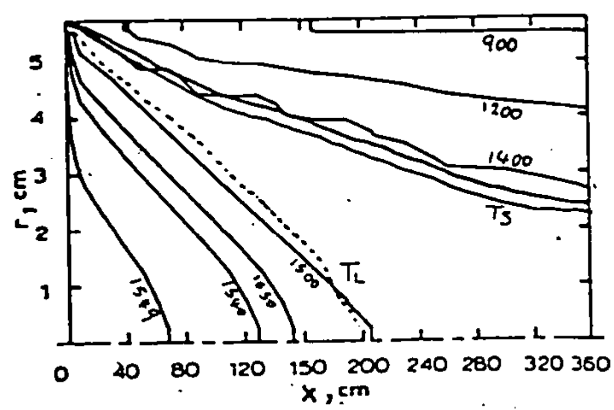

FIG: 4.22-4 COMPUTED TEMPERATURE PROFILE FOR THE TEST OF THE ENERGY EQUATION SOLUTION ALGORITHM

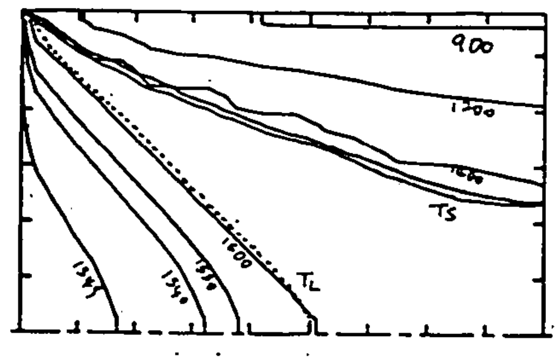

FIG: 4.23-1 COMPUTED TEMPERATURE PROFILE FOR THE CASE OF VARIABLE THERMOPHYSICAL PROPERTIES

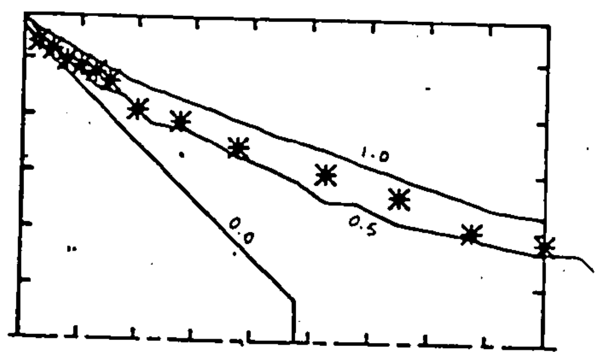

FIG: 4.23-2 COMPUTED SOLID FRACTION DISTRIBUTION FOR THE CASE OF VARIABLE THERMOPHYSICAL PROPERTIES

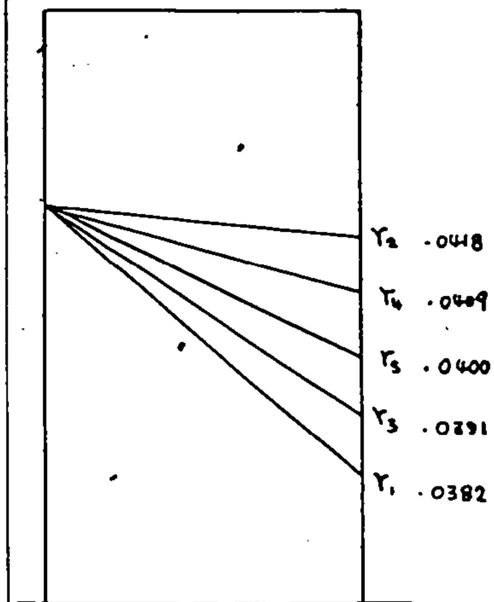

FIG: 4.24-1a A SECTION AT X = 1 cm. WITH VARIOUS GUESSED LOCATION OF SOLIDUS LINE

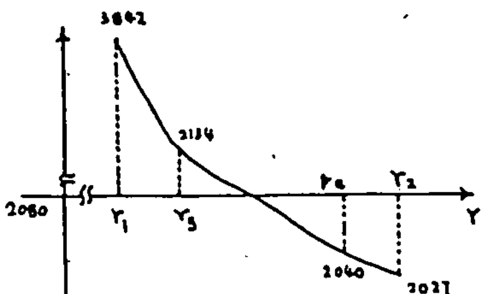

FIG: 4.24-1b PLOT OF COMPUTED Qcool VS RADIAL DISTANCE r

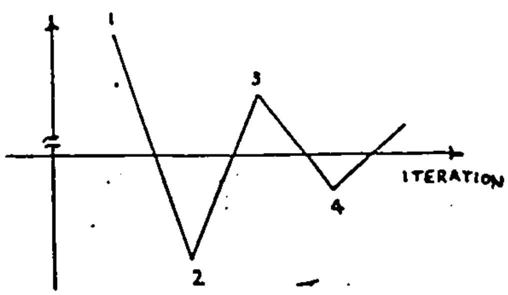

FIG: 4.24-1c PLOT OF COMPUTED Qcool VS NUMBER OF ITERATION

SIMPLIFIED DIAGRAMS TO ILLUSTRATE THE LINE TRACE PROCEDURE AT X = 16.0 cm. (NOT TO SCALE)

FIG: 4.24-1 SOLIDUS LINE TRACING PROCEDURE FOR A SECTION OF DOMAIN AT X = 16 cm

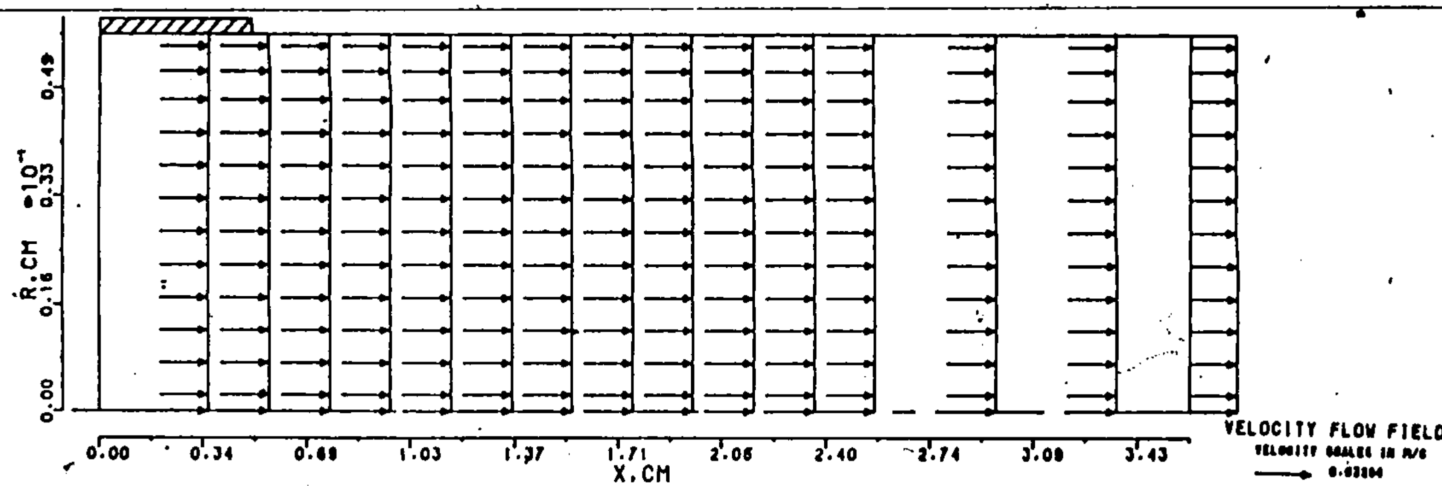

FIG: 4.32-1a COMPUTED AXIAL-VELOCITY PROFILES AT VARIOUS AXIAL POSITIONS (LAMINAR CASE)

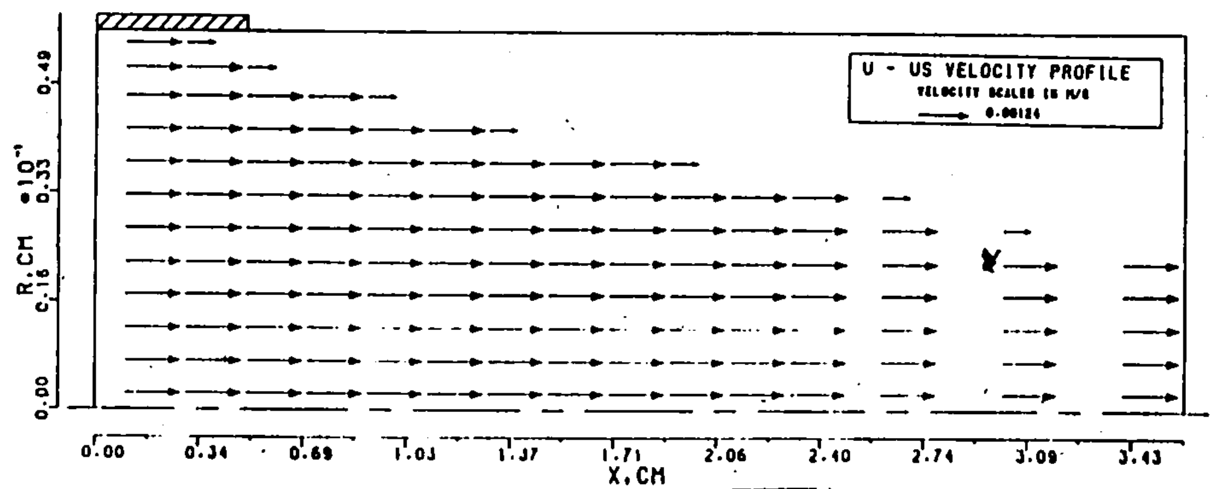

FIG: 4.32-1b COMPUTED VELOCITY FIELD, RELATIVE TO THE CASTING SPEED (LAMINAR CASE)

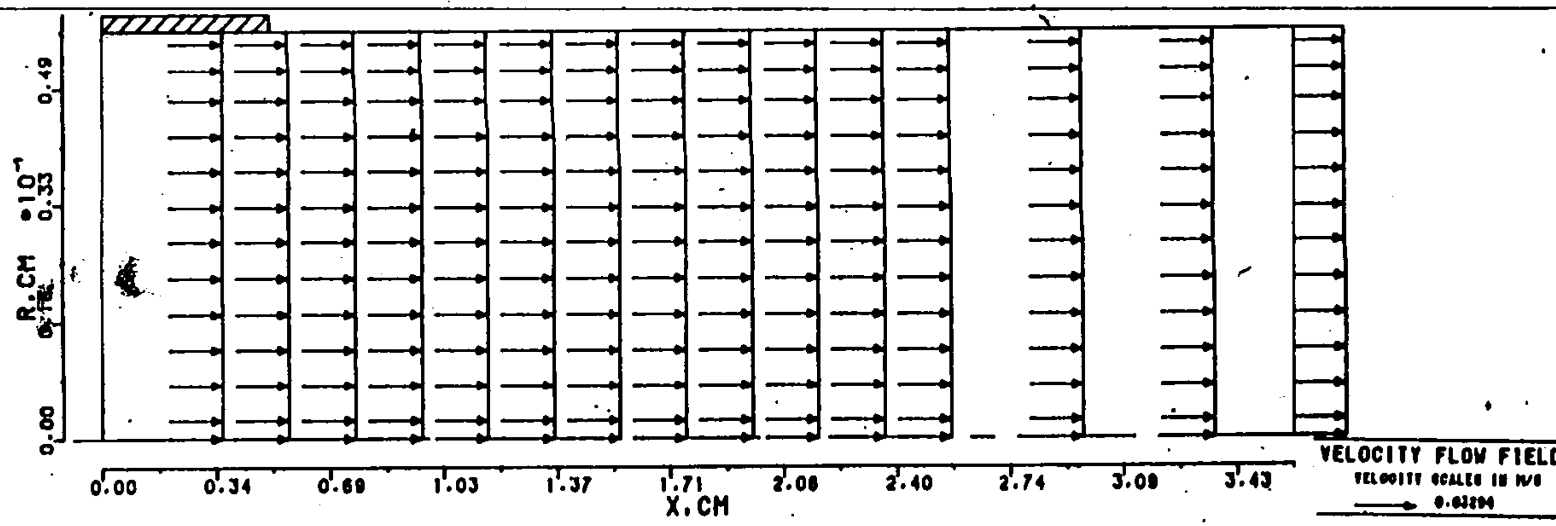

FIG: 4.32-1c COMPUTED AXIAL-VELOCITY PROFILES AT VARIOUS AXIAL POSITIONS (TURBULENT CASE)

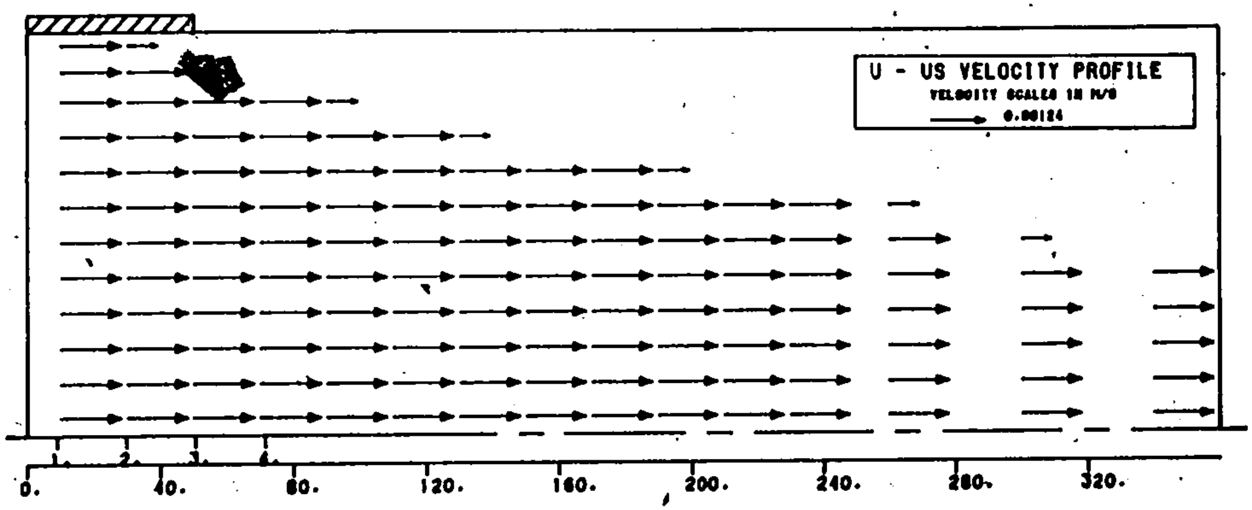

FIG: 4.32-1d COMPUTED VELOCITY FIELD, RELATIVE TO THE CASTING SPEED (TURBULENT CASE)

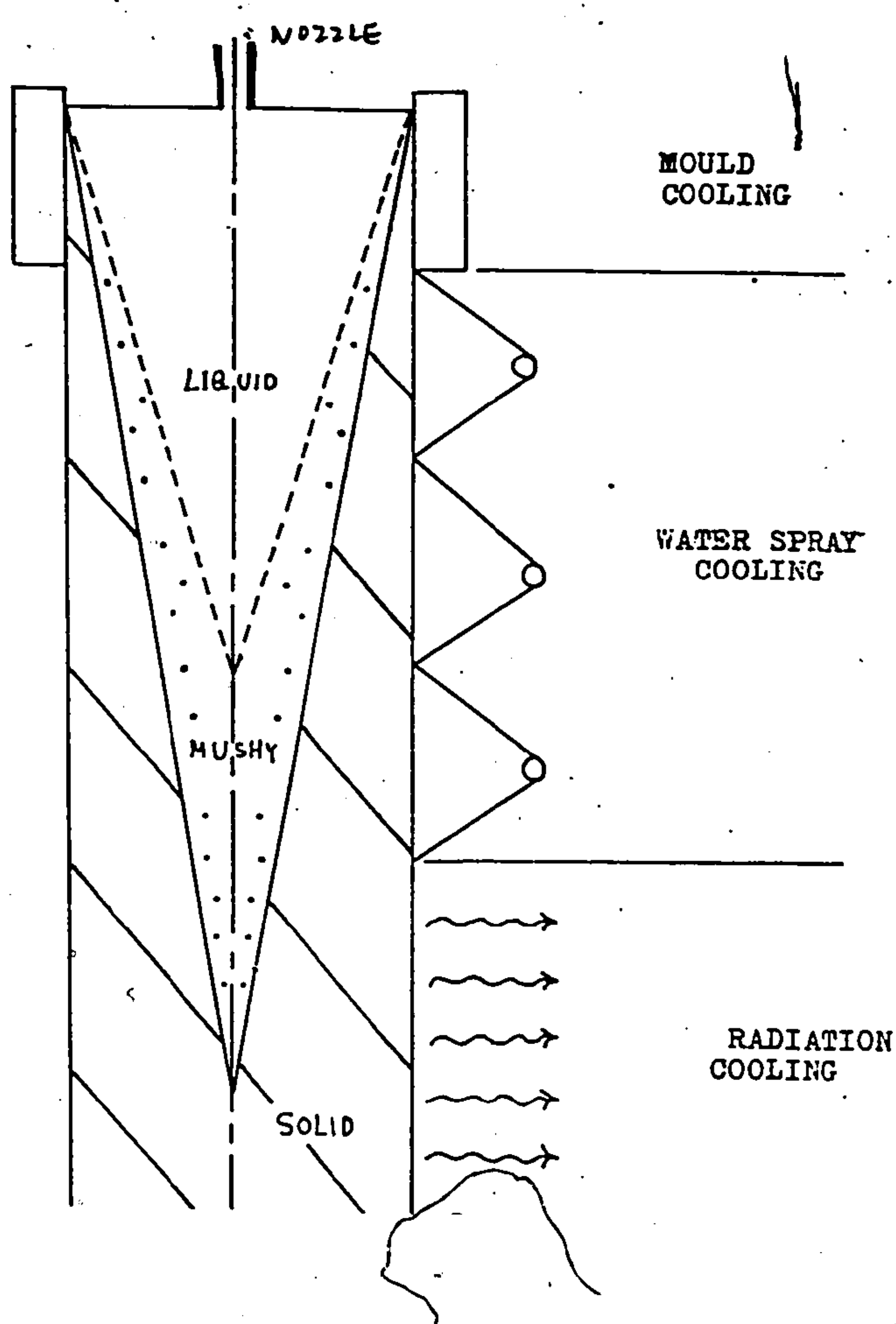

FIG: 4.33-1 THE PHYSICAL SITUATION FOR A NOZZLE CONFIGURATION

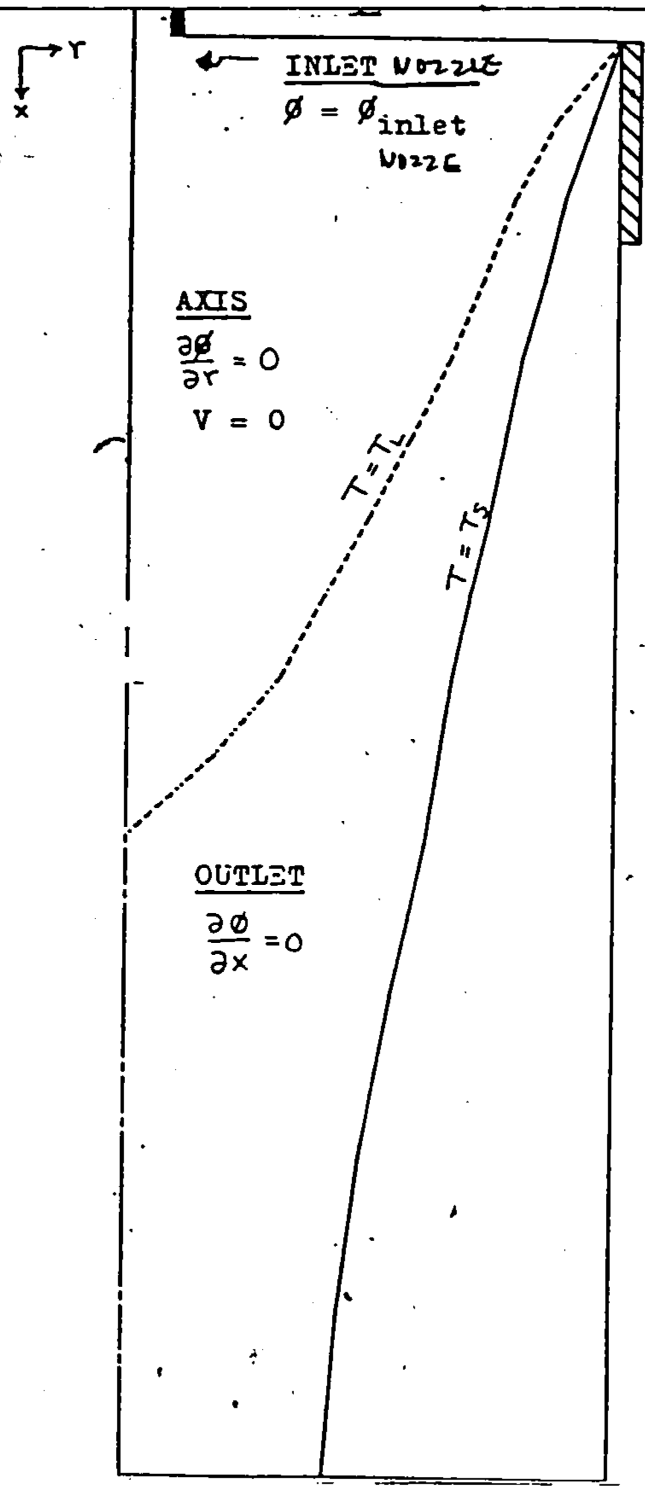

FIG: 4.33-2 THE DOMAIN OF SOLUTION AND THE BOUNDARY CONDITIONS FOR A NOZZLE CONFIGURATION

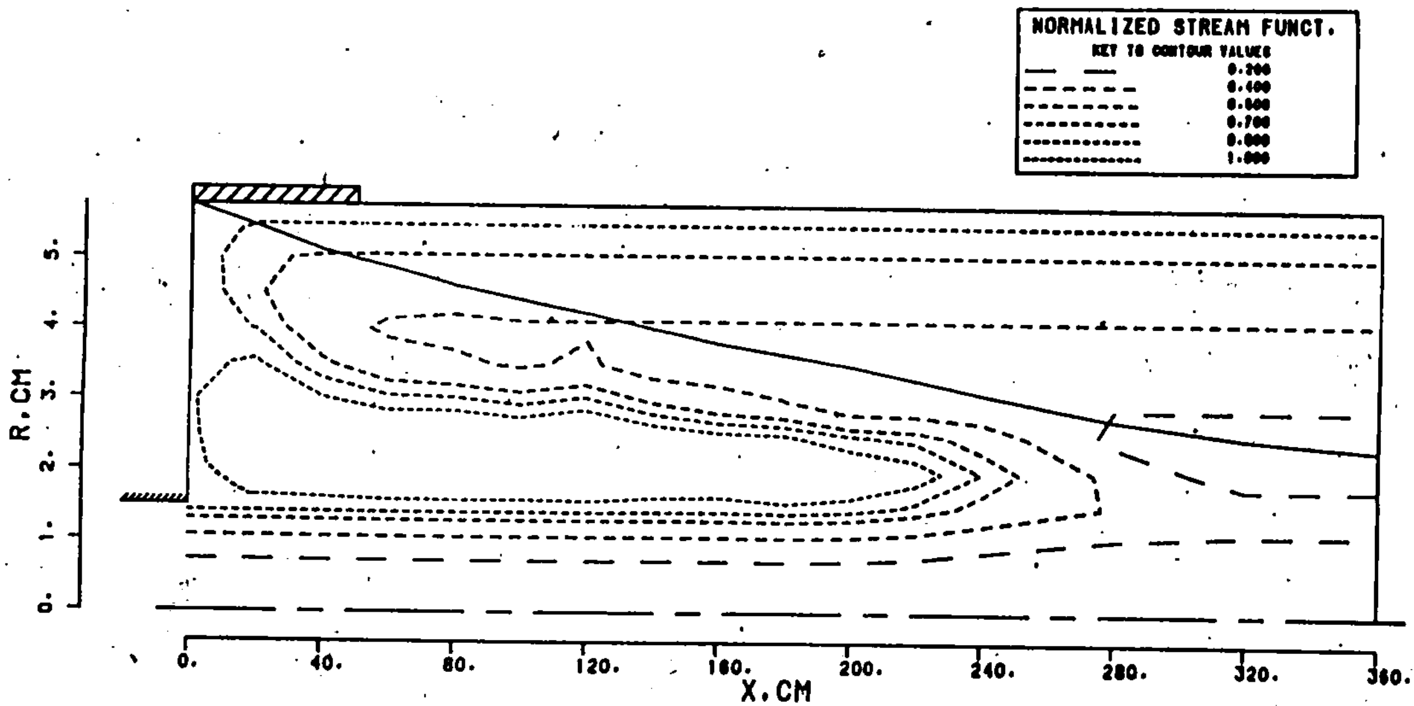

FIG: 4.33-3a COMPUTED NORMALIZED STREAMLINE PATTERN

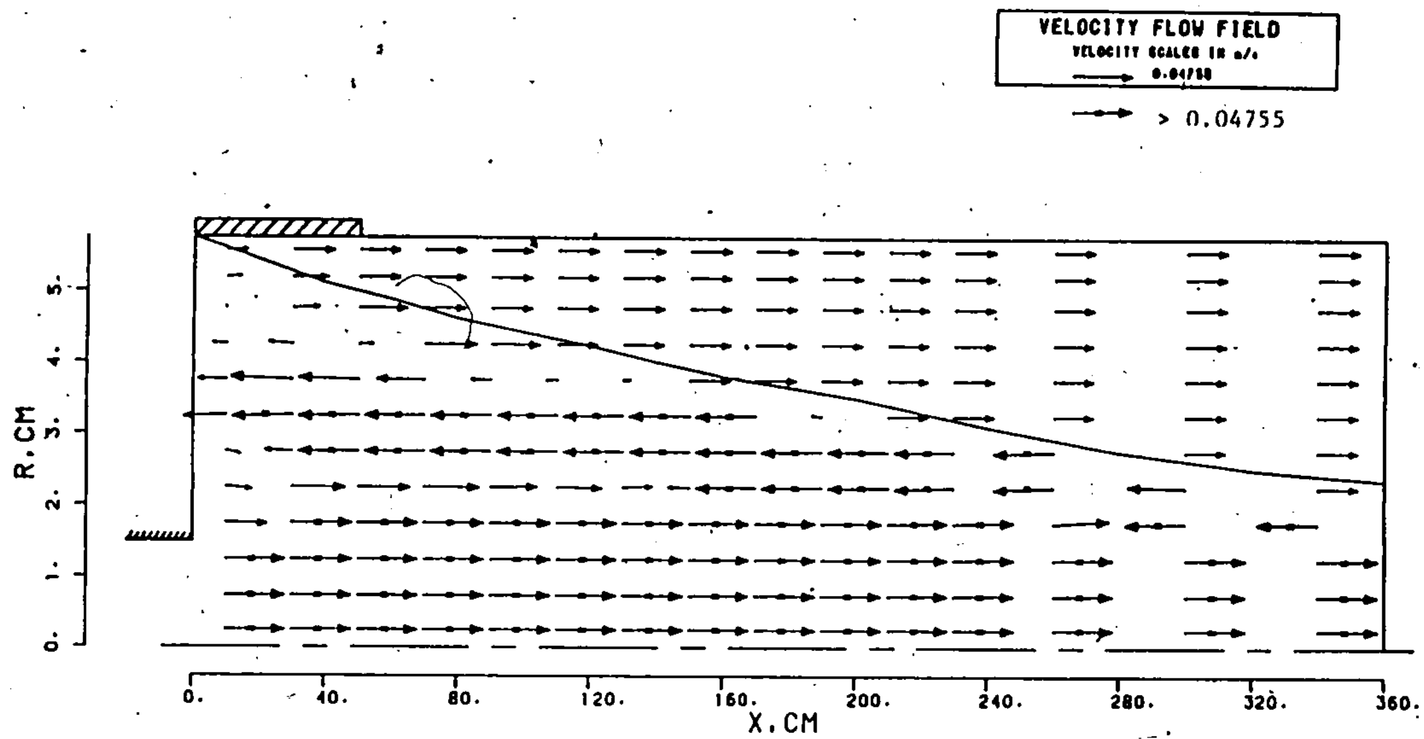

FIG: 4.33-3b COMPUTED VELOCITY FIELDS FOR A NOZZLE CONFIGURATION

COMPARISION WITH EXPERIMENT

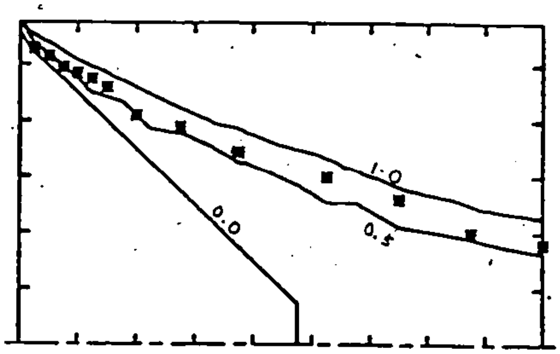

COMPARISON OF COMPUTED PROFILE OF SOLID FRACTION WITH EXPERIMENTAL MEASUREMENT OF SHELL THICKNESS. OBTAINED BY USHIJIMA
(* ⇒ F_s = 0.5)

FIG: 4.42-1 COMPARISON OF COMPUTED PROFILES OF SOLID FRACTION WITH EXPERIMENTAL MEASUREMENTS OF SHELL THICKNESS OBTAINED BY USHIJIMA

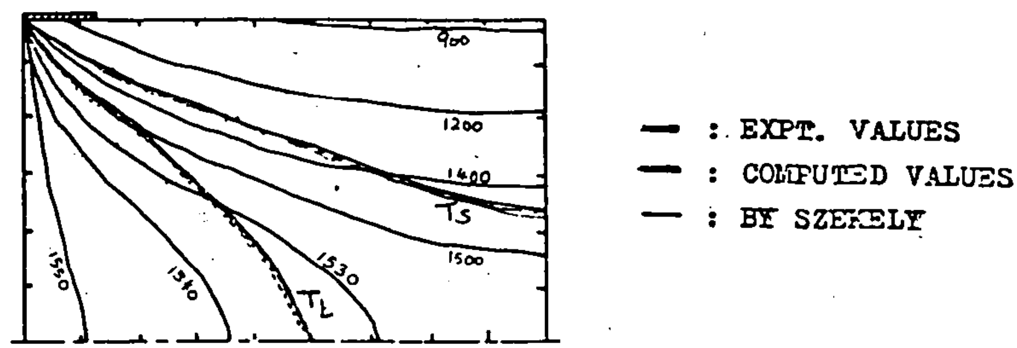

FIG: 4.43-1 COMPARISON OF COMPUTED TEMPERATURE PROFILES BY PRESENT MODEL WITH PREDICTIONS OF PREVIOUS WORK

APPENDIX 1

EXPRESSIONS OF VOLUME RATIO θ

Two Generalized Expressions :

$$\theta_\zeta = 1 - 1/2\{ (1-\gamma_e)[(1-\gamma_n)+(1-\gamma_s)] + (1-\gamma_w)[(1-\gamma_n)+(1-\gamma_s)]\}_\zeta \qquad (3.23\text{-}21)$$

$$\theta_\zeta = [1/2(\gamma_e+\gamma_w)(\gamma_n+\gamma_s)]_\zeta \qquad (3.23\text{-}20)$$

where $\zeta = 1$ or so

(i) All $\gamma_{1,\xi} = \gamma_{so,\xi} = 0$ where $\xi = e, w, n$ or s

$\theta_1 = \theta_{so} = 0$

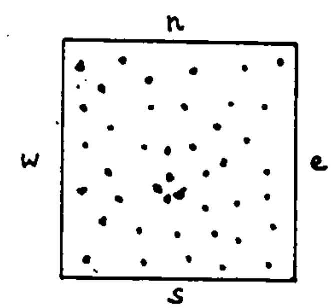

(ii) All $\gamma_{1,\xi} \neq 0$

For Liquid Region :

$\theta_1 = 1 - (\theta_m + \theta_{so})$

$1 - \Delta abc$

$1 - 1/2(ac)(ab)$

$1 - 1/2\{(1-\gamma_e)(1-\gamma_n)\}_1$

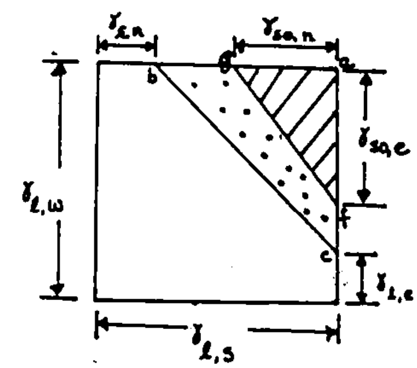

Note : For definition of notations, see page 125

Since $\gamma_{1,w} = \gamma_{1,s} = 1$

$$\theta_1 = 1 - 1/2 \{(1 - \gamma_e)[(1 - \gamma_n) + (1 - \gamma_s)] + (1 - \gamma_w)[(1 - \gamma_n) + (1 - \gamma_s)] \}_1$$

= expression 3.23-21

For Solid Region :

$$\theta_{so} = \Delta afg$$

$$= 1/2(af) (ag)$$

$$= 1/2(\gamma_{so,e}) (\gamma_{so,n}).$$

Since $\gamma_{so,w} = \gamma_{so,s} = 0$

$$\theta_{so} = 1/2 [(\gamma_e + \gamma_w) (\gamma_n + \gamma_s)]_1 .$$

= expression 3.23-20

(iii) All $\gamma_{so,\xi} \neq 0$

Derivation is similar as in case (ii)

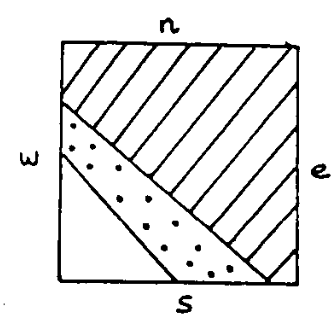

(iv) Not all $\gamma_{\zeta,\xi} \neq 0$

For Liquid Region :

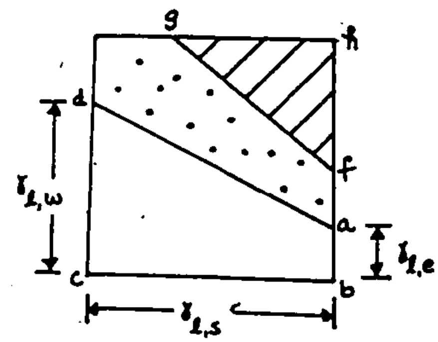

θ_1 = Trapezoid abcd

= 1/2(ab + cd) (bc)

= $[1/2(\gamma_e + \gamma_w)(\gamma_s)]_1$

Since $\gamma_{1,n} = 0$

$\theta_1 = [1/2(\gamma_e + \gamma_w)(\gamma_n + \gamma_s)]_1$

= expression 3.23-20

For Solid Region :

$\theta_{so} = \Delta hfg$

= expression 3.23-20

Derivation is the same as in case (ii)'s solid region

Notations :	
Subscript	Definition
1	liquid
m	mushy
so	solid

BIBLIOGRAPHY

1. Adams C.M., Proc.seminar, Liquid Metals and Solidification, 39th National Metal Congress. Chicago: America Society of Metals, 1957.

2. Allen, H.E. et al, "Continuous Casting of Steel", The Metals Society, London, pp. 215, 1977; Marsh J. and Toothill, ibid., pp. 209.

3. Amsden A.A. and Haarlow F.H., "The SMAC method: A Numerical Technique for Caculating Incompressible Fluid Flows". Los Alamos Scientific Laboratory, LA-4370, Feb., 1970.

4. Asai S. and Szekely J., "Turbulent Flow and Its Effects in Continuous Casting", Iron.Steelmaking, No.3, 1975, pp. 205.

5. Bird R.B., Stewart W.E. and Lightfoot E.N., "Transport Phenomena", New York: Wiley, 1960.

6. Bode C.H. et al, "Continuous Casting of Steel". Londaon: The Metals Society, 1977, pp. 75.

7. Brody H.D. and Stoehr R.A., "Computer Simulation of Heat Flow in Casting". Journal of Metals, Sept.,1980.

8. Chorin A.J., "Numerical Solution of the Navier-Stokes Equations". Math. Comp., 22, pp. 745.

9. Eckert E.R.G. and Drake R.M., "Heat and Mass Transfer". McGraw Hill, 1959.

10. Garcia A. and Prates M., "Mathematical Model for the Unidirectional Solidification if Metals: I. Cooled Models". Met. Trans. B., 1978, Vol. 9B, pp. 449.

11. Garcia, Clyne and Prates, "Mathematical Model for the Unidirectional Solidification of Metals. II. Massive Moulds". Met. Trans., Vol. 10B, 1979, pp. 85-92.

12. Gentry R.A., Matin R.E. and Daly B.J., "An Eulerian Differencing Method or Unsteady Compressible Flow Problems". J. Comp. Phys. 1, 1966, pp. 87-118.

13. Gosman A.D. and Iderish F.D.K., "TEACH-2E: A General Computer Programme for Two-Dimensional Turbulent Recirculating Flow". Dept. of Mech. Eng., Imperial College, Univ. of London, 1976.

14. Gosman A.D., et al. <u>Heat and Mass Transfer in Recirculating Flows</u>. London and New York, Academic Press, 1969.

15. Harlow F.H. and Welch J.E., "Numerical Calculation of Time-dependent Viscous Incompressible Flow Of Fluid With Free Surface". Physics Fluids 8, 1965, 2182.

16. Hills A.D., JISI, 203, 1965, 18.

17. Hills A.D., Trans. Met. Soc. AIME, 245, 1969, 1471.

18. Hills A.W.D., "simplified Theoretical Treatment for the Transfer of Heat in Continuous Casting Machine Moulds". Journal. Iron Steel Inst., Vol. 203, 1965, pp. 18-26.

19. Householder A.S. (1964), "The Theroy of Matrices in Numerical Analysis". New York: Blaisdell.

20. Ideriah F.J.K., "Turbulent Natural And Force Convection In Plumes And Cavities". PhD Thesis, University of London, 1977.

21. Jones W.P. and Launder B.E., "The Prediction of Laminarization with a 2-Equation Model of Turbulence". Int. J. Heat and Mass Transfer, Vol. 15, 1972, pp. 301.

22. Kung E.Y. and Pollock J.C., "Instrumentation for the Iron and Steel Industry". ISA proceedings, 17, 1967, 8.

23. Lai K.Y.M., "Numerical Analysis of Fluid Transport Phenomena". PhD Thesis, University of Londaon, 1983.

24. Lait J.E., Brimacombe J.K. and Weinberg F., "Mathematical Modelling of Heat Flow in the Continuous Casting of Steel". Ironmaking and Steelmaking, No.2, 1974, pp. 90.

25. Launder B.E. and Spalding D.B., "Mathematical Models of Turbulence". London and New York: Academic Press, 1972.

26. Launder B.E. and Spalding D.B., "The Numerical Computation of Turbulent Flows". Computer Methods in Applied Mechanics and Engineering, Vol. 3, 1974, pp. 269.

27. Lightfoot N.M.H., J. Iron Steel Inst., Vol. 119, 1929, pp. 364.

28. Lightfoot N.M.H., J. Iron Steel Inst., Vol. 2, 1932, pp. 162.

29. Marrone R.E., Wilkes J.O. and Pehlke R.D., "Numerical Simulation of Solidification. Part I: Low Carbon Steel Casting- "T" Shape". AFS Cast Metals Research Journal, Dec.,1970, pp. 184.

30. Miyazawa K. and Muchi I., "Mathematical Model for Determining Solidification Profiles of Slab in the Vertical Type and the Circular-arc Type Continuous Casting Machines". Transactions ISIJ, Vol. 15, 1975, pp. 37.

31. Mizikar E.A., "Mathematical Heat Transfer Model for Solidification of Continuously Cast Steel Slabs". Transactions of the Metallurgical Society of AIME, Vol. 239, Nov.,1967, pp. 1747.

32. Moin P. and Kim J., "Large-Scale Numerical Simulation of Wall Bounded Turbulent Shear Flows". NASA TM-81309, 1981.

33. Moriyama A. and Muchi I., Testu-to-Hagane, 55, 1969, 682.

34. Morton S.K. and Weinberg F., "Continuous Casting of Steel. Part I. Pool Profile, liquid Mixing and Gas Structure in the Continuous Casting of Mild Steel". J. Iron Steel Inst., Vol. 211, 1973, pp. 13-23.

35. Patankar, S.V. and Spalding, D.B., "A Calculation Procedure for Heat, Mass and Momentum Transfer in Three-Dimensional Parabolic Flows". Int J. Heat Mass Transfer, Vol. 15, 1972, pp. 1787.

36. Patankar S.V., "Numerical Heat Transfer and Fluid Flow". New York: McGraw-Hill Book Company, 1980.

37. Peel D.A. and Pengelly A.E., "Mathematical Models in Metallurgical Process Development". London: The Iron and Steel Institute, 1970.

38. Pehlke R.D., Metals Eng. Quart., Vol. 4, No. 2, 1964, pp 42-47.

39. Reynolds W.C. and Perkins H.C., Engineering Thermodynamics. 2nd ed. McGraw-Hill Book Company, 1977.

40. Rodi W., "Turbulence Models and Their Application in Hydraulics- A State of the Art Review". University of Karlsruhe, 1980.

41. Rogallo R.S., "Numerical Experiments in Homogeneous Turbulence". NASA TM-81315, Sept.,1981.

42. Savage J., J. Iron Steel Inst., Vol. 200, 1962, pp. 41-7.

43. Savage J, and Pritchard W. H., JISI, 178, 1954, 267.

44. Scheidegger A.E., The Physics of Flow Through Porous Media. New York: Macmillan Press, 1960, pp. 116.

45. Spalding D.B., "A Novel Finite-Difference Formulation for Differential Equation Involving Both First and Second Derivatives". Int. J. Numerical Methods in Engineering, Vol. 4, 1972.

46. Stewart M.J. and Weinberg F., Metall. Trans., Vol. 3, 1972, pp. 333.

47. Szekely J. and Jassal A.S., "An Experimental and Analytical Study of the Solidification of a Binary Dendritic System". Metall. Trans. B, Vol. 9B, 1978, pp. 389.

48. Szekely J. and R.T. Yadoya, Metall. Trans., Vol. 4, 5, 1973, pp. 1379.

49. Szekely J. and Todd M.R., Int. Heat and Mass Transfer. Vol. 14, 1971, pp. 467-82.

50. Touloukian Y.S., "Thermophysical Properties of Matter". Thermophysical Properties Research Centre. Purdue University, 1970.

51. Townsend A.A., "The structure fo Turbulent Shear Flow", Cambridge University Press, 1956.

52. Ushijima, Tetsu-to-Hagane, 48, 6, 1962, 747.

53. Vandrunen G., Brimacombe J.K., Weinberg F., Iron.Steelmaking, No. 2, 1975, pp. 125, 175.

54. Voller V. and Cross M., "An Explicit Numerical Method to Track A Moving Phase Change Front". Int. J. Mass Transfer, Vol.26, No.1, 1983, pp. 147-150.

55. Weckman D.C., Pick R.J. and Niessen P., "A Numerical Heat Transfer Model of the D.C. Continuous Casting Process". Z.Metallkde, 11, 1979, pp. 750.

56. Weinberg, F. "The Casting of Steel", Metall. Trans. A, Vol. 6A, pp. 1971, 1975.

57. Yadoya R.T., PhD thesis, "A numerical Model and a Hydraulic Analog for the Behaviour of the Liquid Core in Continuous Casting of Steel". State University of New York, Buffalo, 1972.